5-2016

Computational Investigation of Impingement Cooling for Regeneratively Cooled Rocket Nozzles

Bianca A. De Angelo

COMPUTATIONAL INVESTIGATION OF IMPINGEMENT COOLING FOR REGENERATIVELY COOLED ROCKET NOZZLES

A Thesis

Submitted to the Faculty

of

Embry-Riddle Aeronautical University

by

Bianca A. De Angelo

In Partial Fulfillment of the

Requirements for the Degree

of

Master of Science in Aerospace Engineering

May 2016

Embry-Riddle Aeronautical University

Daytona Beach, Florida

COMPUTATIONAL INVESTIGATION OF IMPINGEMENT COOLING
FOR REGENERATIVELY COOLED ROCKET NOZZLES

by

Bianca A. De Angelo

A Thesis prepared under the direction of the candidate's committee chairman, Dr. Mark Ricklick, Professor, Department of Aerospace Engineering, and has been approved by the members of the thesis committee, Dr. Eric Perrell and Dr. Habib Eslami. It was submitted to the School of Graduate Studies and Research and was accepted in partial fulfillment of the requirements for the degree of Master of Science in Aerospace Engineering.

THESIS COMMITTEE

Chairman, Dr. Mark Ricklick

Member, Dr. Eric Perrell

Member, Dr. Habib Eslami

Department Chair, Dr. Anastasios Lyrintzis
or Graduate Program Coordinator, Dr. Eric Perrell

27 April 2016
Date

Dean of College of Engineering, Dr. Maj Mirmirani

4/28/2016
Date

Vice Chancellor, Academic Support, Dr. Christopher Grant

4/28/16
Date

ACKNOWLEDGMENTS

I would first and foremost like to thank my advisor, Dr. Ricklick, for the countless hours he has given me throughout my time at Embry-Riddle. Your enthusiasm and extensive knowledge have taught me a great deal beyond the classroom. You have helped me to stay focused and further pursue my desire to work within aerothermal analysis and testing. You've helped to bring out the engineer in me, not just the physicist. Over the years, you've not only helped answer my *many* questions, but believed in me and pushed me to excel within my graduate career. I am forever thankful for everything that you have done for me. I truly could not have asked for a better thesis advisor.

Additionally, I would like to thank everyone who has helped me along this journey. To my committee members, Dr. Perrell and Dr. Eslami: thank you for putting in the time and effort to ensure my thesis is one I am proud to have for the rest of my life. To the Propulsion Thermal Management Laboratory (PTML) and Gas Turbine Laboratory (GTL): thank you to all my friends and lab mates for the endless support and encouragement. From our conversations and countdowns, laughs, long nights, and countless coffee runs with the "Caffeine Addicted Grads", you have all made my time here memorable.

Lastly, I would like to thank my family for the endless support they have given me. You have always been there for me, from daily phone calls to talk about thesis or life. You have always been the support I needed after a long day of research. Although being hundreds of miles away these past few years, this time has only brought us closer together in so many ways. Thank you Mama, Papa, Franchesca, and Brandon for believing in me and my dreams —I love you (more), always.

TABLE OF CONTENTS

LIST OF TABLES

LIST OF FIGURES

SYMBOLS

Symbols

A	Area (mm^2)
A_*	Area of Nozzle Throat (mm^2)
Bi	Biot Number
C^*	Characteristic Velocity (m/s)
c_p	Specific Heat at Constant Pressure (J/kg*K)
D	Jet Hydraulic Diameter (mm)
D_*	Nozzle Diameter, at Throat (mm)
Gc	Channel Cross-Flow Mass Flux (kg/m^2)
Gj	Jet Mass Flux (kg/m^2)
g	Gravitational Acceleration (m/s^2)
h	Convective Heat Transfer Coefficient (W/m^2*K)
k	Thermal Conductivity (W/m*K)
L	Characteristic Length (m)
M	Mach Number
m	Slope
$\dot{m}$	Mass Flow Rate (kg/s)
Nu	Nusselt Number
P	Pressure (Pa)
Pr	Prandtl Number
Q	Heat Transfer Rate (W)
q''	Heat Flux (W/m^2)
R	Resistance (m^2*K/W)
Rf	Effective Recovery Factor
Re	Reynolds Number
r	Radial Distance (mm)
rf	Local Recovery Factor
r/D	Radial Distance, in terms of Jet Diameters
S_{ij}	Rate of Strain Tensor
Sc	Schmidt Number
Sh	Sherwood Number
T	Temperature (K or °C)
T_3	Temperature, at Turbine Inlet (K or °C)
t	Time (s)
th	Thickness (m)
V	Volume (m^3)
v	Velocity (m/s)
X	Streamwise Distance (mm)
X/D	Streamwise Distance, in terms of Jet Diameters
Y	Spanwise Distance (mm)
Y/D	Spanwise Distance, in terms of Jet Diameters
Z	Jet Height (mm)
Z/D	Jet Height, in terms of Jet Diameters

Greek Symbols

α	Linear Thermal Expansion Coefficient (1/K)
γ	Ratio of Specific Heats
δ_{ij}	Kronecker Delta
ε	Turbulent Dissipation Rate
μ	Dynamic Viscosity (Pa*s)
μ_{turb}	Eddy Viscosity (Pa*s)
ν	Kinematic Viscosity (Pa*s)
σ	Tensile Strength (Pa)
τ_{ij}	Reynolds Stress Tensor
ω	Exponent of the viscosity-temperate relation
η	Cycle Efficiency
η_{eff}	Film Cooling Effectiveness
ρ	Density (kg/m^3)

Subscripts

0	Stagnation
aw	Adiabatic Wall
c	Curvature
ch	Combustion Chamber
cond	Conduction
conv	Convection
cool	Cool Side
fluid	Fluid
g	Hot Gas
hot	Hot Side
jet	Hydraulic Jet
max	Maximum Value
melt	Melting
min	Minimum Value
solid	Solid Body
stag	Stagnation Point
tot	Total
wall	Wall

ABBREVIATIONS

1-D	One-Dimensional
2-D	Two-Dimensional
3-D	Three-Dimensional
ABS	Acrylonitrile Butadiene Styrene
ARN	Array Round Nozzle
ASN	Array Slot Nozzle
CD	Convergent-Divergent
CEA	Chemical Equilibrium with Applications
CFD	Computational Fluid Dynamics
CHT	Conjugate Heat Transfer
DNS	Direct Numerical Solution
EBkε	Elliptic-Blending Kinetic Energy
Imp.	Impingement
LES	Large Eddy Simulation
LH2	Liquid Hydrogen
LOX	Liquid Oxygen
LPRE	Liquid Propellant Rocket Engine
NIST	National Institute of Standards and Technology
RANS	Reynolds-Averaged Navier-Stokes
Rkε	Realizable Kinetic Energy
STAR-CCM+	Simulation of Turbulence in Arbitrary Regions-Computational Continuum Modeling
SRN	Single Round Nozzle
SS	Stainless Steel
SSME	Space Shuttle Main Engine
SSN	Single Slot Nozzle
TBC	Thermal Barrier Coating
TKE	Turbulent Kinetic Energy
TSP	Temperature Sensitive Paint
v^2f	Normal Velocity Relaxation Model

NOMENCLATURE

°C	Degree Celsius
1/K	One per Kelvin
GPa	Giga-Pascal
J/kg*K	Joule per Kilogram Kelvin
K	Degree Kelvin
kg	Kilogram
kg/m^2	Kilogram per Meter Squared
kg/m^3	Kilogram per Meter Cubed
kg/s	Kilogram per Second
kN	Kilo-Newton
m	Meters
m/s	Meter per Second
m^2*K/W	Meters Squared Kelvin per Watt
m^3	Meters Cubed
mm	Millimeters
mm^2	Millimeters Squared
MPa	Mega-Pascal
Pa	Pascal
Pa*s	Pascal Second
s	Seconds
W	Watt
W/m*K	Watts per Meter Kelvin
W/m^2	Watts per Meter Squared
$W/m^{2*}K$	Watts per Meters Squared Kelvin

ABSTRACT

Researcher: Bianca A. De Angelo

Title: Computational Investigation of Impingement Cooling for Regeneratively Cooled Rocket Nozzles

Institution: Embry-Riddle Aeronautical University

Degree: Master of Science in Aerospace Engineering

Year: 2016

Jet impingement cooling is an internal cooling configuration used in the thermal management of temperature sensitive systems. With rocket engine combustion temperatures rising as high as 3600 K, it is essential for a cooling method to be applied to ensure that the nozzle integrity can be maintained. Therefore, a novel heat transfer study is conducted to investigate if jet impingement cooling is feasible for a regenerative cooling rocket nozzle application. Regenerative cooling for liquid propellant rockets has been widely studied. However, to the best of the author's knowledge, there is currently no literature describing this method in conjunction with impingement cooling techniques.

In this study, a literary empirical model by Martin (1977) is compared to a computational fluid dynamics (CFD) model designed for single round nozzle (SRN) jet impingement with conjugate heat transfer (CHT) analysis. The CHT analysis is utilized to investigate the resulting surface temperatures in the presence of convection and lateral conduction effects while investigating the Nusselt number (Nu) and temperature profiles of the impingement configuration. Heat transfer data is first extracted for air impinging onto a heated flat plate, whose results are used as the benchmarking model.

The model is then altered to assess its application feasibility for a regeneratively

cooled rocket nozzle throat similar to that of the Space Shuttle Main Engine (SSME) with LOX/LH2 propellants. A 1-D thermal analysis of supercritical LH2 coolant at 52.4 K and 24.8 MPa for the SSME with various nozzle wall materials, such as Stainless Steel 304 (SS 304), Inconel x-750, copper and ABS plastic, is conducted. The material selections were chosen to cover a range of thermal conductivities. It was found that none of the selected materials are feasible with impingement cooling alone due to the extremely high heat transfer rates within the throat.

With material temperature limitations below 2000 K, the materials cannot withstand the high stresses acting on the nozzle even with alterations to the benchmark model. Therefore, it is concluded that an additional cooling method is required to increase the hot-side thermal resistance. To ease the thermal stresses on the remaining metals, an average film cooling effectiveness (η) of 0.5 was assumed, to simulate the benefit of film cooling. Having been incorporated into the hot gas side calculations, it decreased the adiabatic wall temperature from 3561 K to 1667.3 K, allowing the materials to be properly cooled on the inner side of the nozzle. Even with this assisted cooling method added, it is concluded that only SS 304 and Inconel x-750, with their low material resistance and high temperature capabilities, were capable of withstanding the rocket nozzle temperatures. CFD simulations for these two materials are studied for their feasibility of a SSME-like nozzle throat region. It was concluded that film cooling cannot be eliminated from the system with the SSME parameters studied. Additionally, with minimal differences between the 1-D analysis and CFD simulations, lateral conduction effects are minimal, which proves 1-D analysis is sufficient for future analysis.

1. Introduction

1.1. Motivation

With structural and material designs of engine components compromised when their temperature rises beyond safe operating conditions, effective cooling methods must be implemented. Cooling capabilities allow the engine to have an improved performance due to an increased combustor temperature, leading to higher performance and efficiency. This will ultimately improve the engine's fuel economy and power (Zuckerman & Lior, 2006). As a result, heat transfer research has been focused to refine the internal cooling techniques for both gas turbine and rocket engines.

The need for advanced cooling techniques necessitates for scientific knowledge to broaden beyond its current methods. With rocket nozzle reaching extremely high combustion temperatures, upwards of 3600 K in the nozzle throat region where the heat load is highest, a cooling method must be implemented (Turner, 2010). Therefore, modeling a Space Shuttle Main Engine (SSME), a jet impingement cooling study with an extension of conjugate heat transfer (CHT) utilizing computational fluid dynamics (CFD) is applied to a regeneratively cooled rocket nozzle throat region. The heat transfer characteristics are analyzed for the potential of improved engine efficiency from the novel cooling application.

1.2. Introduction to Rockets

Modern rocket propulsion began in 1914 when physicist Robert Goddard patented the first liquid-fueled rocket nozzle (Turner, 2010). He paved the way for modern rocketry with his five-section invention, which included a combustion chamber and firing tube

capable of extreme propulsive power (Goddard, 1914). Since then, a variety of propulsive energy rocket systems have been developed and are categorized as either chemical, nuclear or electrical (Taylor, 2009).

Chemical rockets obtain all of their required energy for propellant acceleration from the propellant itself in the form of a fuel-oxidizer combination (Oates, 1988). They can be broken down in to liquid propellant rocket engines (LPREs) and solid rocket motors. Liquid rocket engines have separate thin-walled tanks for the fuel and oxidizer while solid motors have a premixed combination which burns when heated in the combustion chamber (Taylor, 2009).

For all chemical rockets, the hot exhaust gases are made to escape through the jet nozzle at high velocities, which produces thrust. LPREs are advantageous over their solid counterparts for their highly energetic propellants (Oates, 1988). However, a disadvantage is their large mass resulting from the greater amount of liquid needed to cool the engine. With engine combustion temperatures rising over 3000 K from the high-pressure combustion reaction, it is necessary to cool all surfaces that are exposed to the hot gases (Sutton, 2000). The added mass of coolant increases the rocket's overall weight and ultimately its cost.

Treating a rocket as a heat engine, on the molecular level when the chaotic motion of the heated propellant is converted to a high-velocity ordered motion, the fluid itself will expand and cool. Its thermal energy will be converted to kinetic energy in the process (Turner, 2010). Its power cycle describes how the power is derived to feed the propellants to the main combustion chamber.

1.2.1. Materials and Propellants

From the high operating pressures and temperatures of a LPRE, the engine's materials become highly stressed. As a result, their strength rapidly decreases as the temperature increases (Humble *et al.*, 1995). With combustion temperatures around 3000 K, they are typically higher than the melting point of the wall materials, which are mostly below 2000 K (Turner, 2010). To mitigate this problem, smooth, thin-wall materials are most desirable as they will decrease the thermal stresses and high wall temperatures the materials encounter (Sutton, 2003). Additionally, thinner walls can result in a cooler, more lightweight structure overall. The most widely used metal materials today are Stainless Steel (SS) and nickel-based alloys. This is because of their high thermal conductivity (k) and corresponding low thermal expansion coefficients (α) (Hill & Peterson, 1992). Preliminary work is in progress to investigate 3-D printed thermoplastic resin rocket engine components. This is to investigate potential time, weight and cost reductions while still maintaining, or even increasing, overall efficiency.

Liquid bi-propellants have high specific heat values, with the highest from cryogenic propellants (Huzel & Huang, 1992). One common combination is a liquid oxygen (LOX) with liquid hydrogen (LH2) propellant system. However, a downside to using cryogenic propellants is their need to be kept at very low temperatures (Sforza, 2012). Cryogenic propellants have latent heat capacities while enables a phase change to occur without there being a change of temperature (Bergman & DeWitt, 2011). Once their boiling temperatures are exceeded, the density will decrease and add complexity to the system. Despite this, the high performance values resulting from very high rocket exhaust velocities of the LOX/LH2 combination is still widely desirable. The high performance

capabilities of LOX with the low boiling temperature of LH2 makes it a popular choice within LPREs (Sutton, 2000). Other common fuels to use with LOX are RP-1 or kerosene.

1.2.2. Space Shuttle Main Engine

One famous LPRE is the Space Shuttle Main Engine (SSME), which was first designed in 1972 (Sutton, 2003). It is a reusable, high performance, variable thrust bi-propellant engine. Its ingenuity stems from establishing each portion of the system to run at its maximum thrust efficiency and then at a high exhaust velocity where all of the energy released from the propellants is converted into thrust. In doing so, all of the exhaust from the fuel delivery system will pass though the combustion chamber. This is proven to be a highly efficient system if executed at high combustion chamber temperatures (Turner, 2010). However, running at high temperatures incorporate additional concerns for cooling the engine. Using a staged combustion cycle, the SSME burns cryogenic LOX/LH2 propellants which are used within a regenerative cooling system to avoid melting the engine walls. This study will analyze a rocket nozzle with parameters obtained from the SSM while utilizing cryogenic LOX and LH2 propellants.

1.3. Rocket Cooling

As a result of high temperatures, the rocket engine thrust chamber walls must be cooled. This is to prevent the material from surpassing its maximum allowable temperature, which can lead to structural failures (Sutton, 2003). Reducing the hot gas side wall temperature by 50-100 K can result in doubling the chamber life cycle, which is of interest due to the high cost associated with spaceflight manufacturing (Wang *et al.*, 2006).

If all hot spots on the chamber and nozzle walls are to be avoided, the propellant

must be in contact with the wall at every location. Thus, the flow must be smooth and continuous (Turner, 2010). Common LPRE cooling methods used today are film cooling, transpiration cooling, dump cooling and regenerative cooling. Film cooling uses a portion of the liquid propellant and allows the coolant to flow along the inside surface of the combustion chamber to the hot nozzle surface. It assists to reduce the heat transfer to the wall by reducing the hot gas temperature near the wall, with a dominating effect on a reduced total heat flux (Miranda & Naraghi, 2011). The evaporation of this liquid film results in a layer of cool gas between the wall and hot gases passing from the chamber and through the nozzle (Sutton, 2000). Transpiration cooling is a special case of film cooling where the coolant flows through porous chamber walls (Huzel & Huang, 1992). Dump cooling has hollow combustion chamber and nozzle walls with the propellant passing through the cavities. This generates additional thrust in the system from the resulting waste heat of the exhaust gas (Humble *et al.,* 1995).

1.3.1. Regenerative Cooling

Regenerative cooling is an effective cooling method where fuel is made to circulate around the combustion chamber and nozzle as it absorbs heat conducted through the heated interior surface, shown in Figure 1.1. This heated fuel is then used for combustion (Taylor, 2009). Therefore, the exhaust velocity will increase slightly, from 0.1 to 1.5%, as a result of the propellant's heating. This method has resulted in some of the most efficient engines to date since its first demonstration by Wyld in 1938 (Sutton, 2003). For highly pressurized engines, such as the SSME, it has been studied and concluded that a highly effective cooling technique is regenerative cooling as it does not negatively affect the general performance of the engines (Yang, 2004)

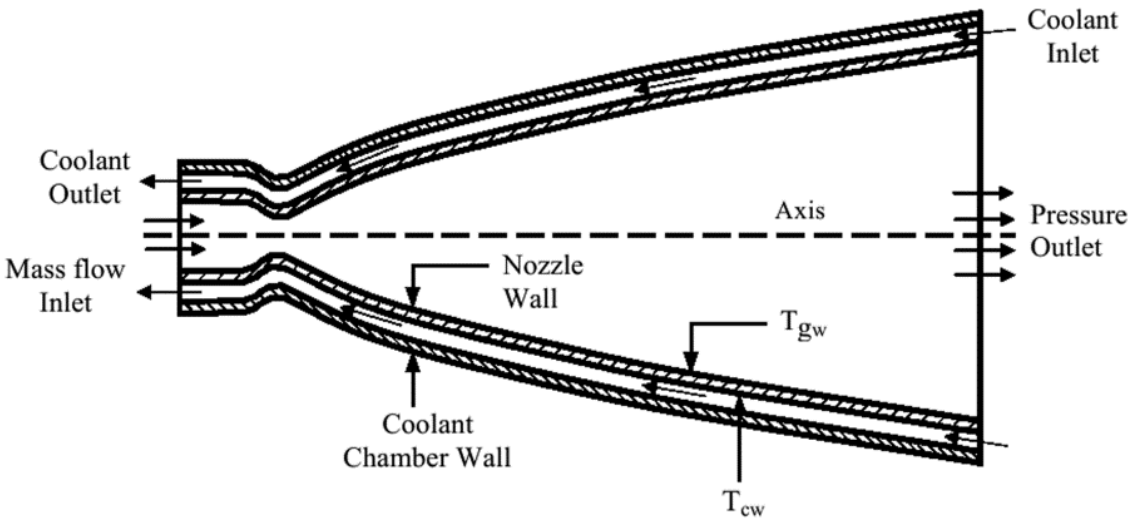

Figure 1.1: Schematic for a Regeneratively Cooled Rocket (Rajagopal, 2015)

This cooling technique is well established for rockets today, however, it still raises concerns due to the large temperature gradients across the combustion chamber walls giving way to large thermal strains. The high wall temperature creates a lifetime limitation for the combustion chamber. Improvements in the heat transfer rates between the combustion chamber wall and coolant will reduce the temperature of the hot gas side wall. This in turn will reduce the stress on the material (Kuhl, 2002). Therefore, the hot gas side heat flux, wall structural requirements, coolant side heat transfer and coolant temperature effects must be analyzed (Huzel & Huang, 1992).

1.4. Rocket Nozzle Heat Transfer

Rocket nozzles produce a steady flow of high velocity gas which flows parallel to the centerline of the nozzle (Sforza, 2012). From the accelerated hot exhaust a thrust is produced along the centerline axis, as displayed in Figure 1.2. Rocket heat transfer analysis is usually completed only for the most critical wall regions such as the nozzle throat, critical chamber locations, and the nozzle exit (Sutton, 2000). The region of the highest heat

transfer occurs at the nozzle throat, where the cross-sectional area is smallest with a Mach number of one (Oates, 1988). As a result, this is the most difficult area to cool.

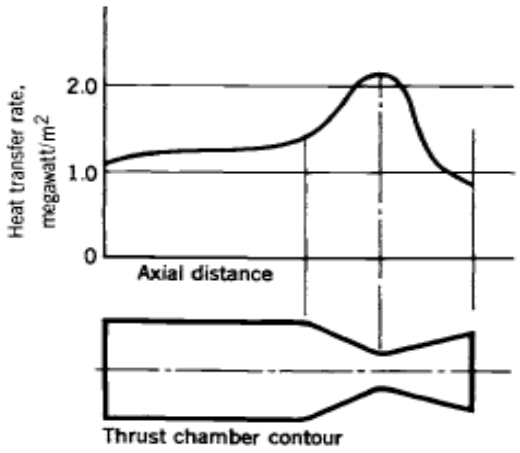

Figure 1.2: Axial Heat Transfer Distribution (Sutton, 2000)

Rocket nozzle heat transfer analysis incorporates all three modes of heat transfer, with a strong emphasis on convection. The heat transfer of a regenerative cooling system consists of a steady heat flow from the hot gas through a solid wall to a cooled liquid (Hill & Peterson, 1992). Using the design parameter values from the combustion chamber, the convective heat transfer can be calculated. When designing a nozzle, the axial heat flux distribution at the nozzle wall is important. A well-known empirical correlation to find the convective heat transfer coefficient (h) was derived by Bartz in 1957. His equations are described in further detail within Chapter 3. Once the hot combustion gas side heat transfer coefficient (h_g) is found, the temperature difference between the adiabatic wall temperature (T_{aw}) of the material and the wall temperature (T_{wall}) is used to calculate the convective heat flux (q''_{conv}) using equation 12 later discussed in sub-section 3.2.1. The adiabatic wall temperature is the driving temperature within these high speed convection problems. As chamber pressures and hot gas wall heat fluxes continue to increase, more effective cooling methods are needed to meet the rocket heat transfer rate demands.

1.5. Introduction to Gas Turbines

For jet engines, their material and hot gas temperatures can rise as high as 1200 to 1600°C respectively. The turbine blades specifically experiences high temperatures (Al-Hadhrami *et al.*, 2011). Therefore, it is essential to keep the blades cooled and the thermal efficiency high. Gas turbine technology has greatly improved over the past few decades to obtain the highest overall cooling effectiveness while having the lowest possible penalty on the thermodynamic cycle performance. Brayton Cycle

Gas turbines operate under the Brayton engine cycle, an open, constant pressure combustion process. Being an open cycle, it has all of its events occurring at the same time but in different locations within the engine (Oates, 1988). The Brayton cycle thermal efficiency is defined below in Equation 1. The maximum temperature, located at the turbine inlet (T_3), is determined by the combustion chamber temperature, which can reach temperatures higher than typical material melting points. Therefore, limiting T_3 is essential for engine material integrity. Thus, for maximum efficiency, T_3 should be as high as possible.

$$\eta = 1 - \frac{(T_4 - T_1)}{(T_3 - T_2)} \quad (1)$$

The ideal Brayton cycle is an isentropic cycle with the assumptions that air behaves as an ideal gas and the temperature rise is a result of the system's combustion process (Moran & Shapiro, 2011). As shown in Figure 1.3, air first enters the inlet at atmospheric pressure and temperature. As it passes through the compressor, the pressure increases. Inside the combustor the air mixes with the engine's fuel and burns while remaining at a constant pressure. However, the temperature increases which causes the volume to also increase. This fluid enters the turbine and expands through it. As the gas passes through

the turbine rotor, the kinetic and thermal energies are converted into mechanical energy for work. The gases are then released though the exhaust where volume drastically decreases (Moran & Shapiro, 2011).

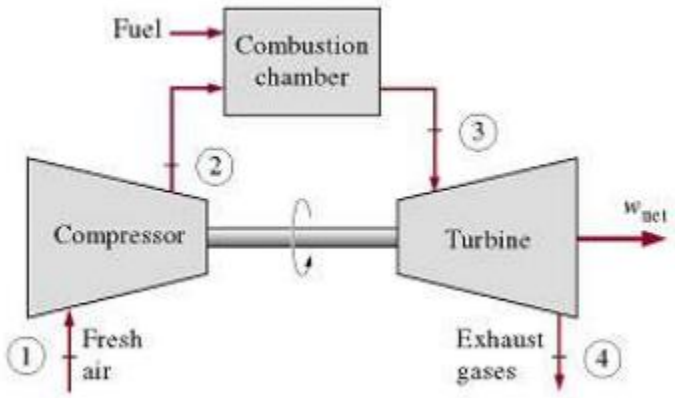

Figure 1.3: Ideal Brayton Cycle (Al-Hadhrami *et al.*, 2011)

1.6. Turbine Blade Cooling

Improved turbine cooling methods have allowed the turbine inlet temperature to increase over the years. However, with increased temperatures, the increased thermal stresses on the blades must also be monitored. Material advancements over the past 50 years have enabled turbine firing temperatures to be increased by approximately 195°C, equivalent to ~4°C per year. Within the same time period, cooling developments have allowed gas temperatures to increase by an additional 11°C per year (Boyce, 2006). Increasing this temperature allows for a more powerful and efficient system. Therefore, accurately predicting the local heat transfer coefficients and metal temperatures is essential.

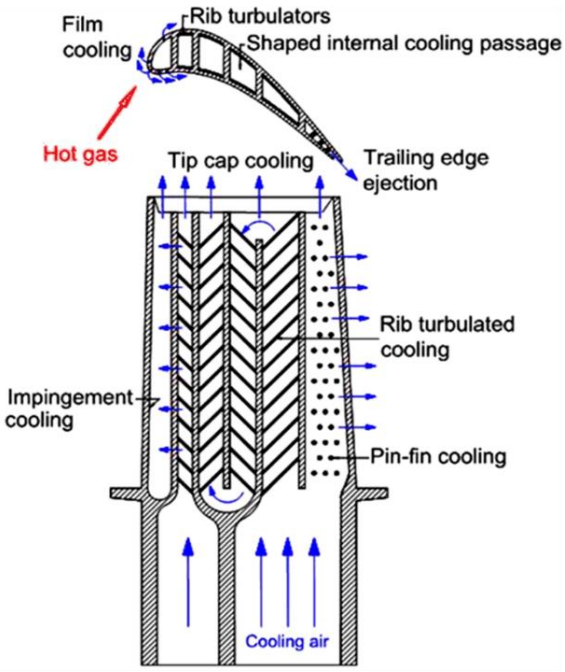

Figure 1.4: Internal Cooling Techniques for Turbine Blades (Han *et al.*, 2001)

Blade cooling techniques can be separated into two categories, external or internal. External cooling is primarily film cooling, and internal cooling incorporates convective cooling methods for the entire turbine blade. The internal cooling techniques are displayed in Figure 1.4 above. At the leading edge, which is the area of the highest heat transfer in turbine blades, there are impingement holes which allow the cool fluid to enter the blade (Ligrani *et al.*, 2003). It is implemented at the blade's leading edge due to its significant potential to increase local heat transfer coefficients (Han *et al.*, 2001). In turn, this temperature reduction boosts overall efficiency. Across the mid-chord region are rib turbulators, and at the trailing edge are pin fins.

1.6.1. Impingement Cooling

Impingement cooling is an internal cooling method which impinges high velocity coolant onto a surface (Han *et al.*, 2001). It is an aggressive cooling technique widely used within gas turbine cooling since the 1960s (Downs & Landis, 1992). Impingement nozzle orifices can be a variety of shapes and configuration combinations. The primary fluid parameter for impingement analysis is the jet Reynolds number (Re_{jet}), based on the orifice diameter (D) and exit velocity (v). The main geometric parameters are the jet-to-target spacing (Z/D), and the jet-to-jet spacing (X/D, Y/D), when applicable in array configurations. With increased values of the jet Reynolds number, increased heat transfer rates are produced (Han *et al.*, 2001).

Shown in Figure 1.5, when a single round nozzle (SRN) jet comes into contact with a heated solid surface, the axisymmetric fluid flows downward and radially outwards within the jet stagnation region. Here, a potential core region can develop with a length up to 4 to 6 times the jet diameter length. As the jet centerline turbulence increases with increasing height, the flow mixing length simultaneously increases and a decrease in stagnation Nusselt number occurs (San & Shiao, 2006). The fluid loses its axial velocity and as a result, is no longer uniform. It will experience both higher normal and shear stresses (Zuckerman & Lior, 2006). Increasing its radial distance from the stagnation region, it enters the wall jet region where a thin, highly turbulent boundary layer is produced. Its thickness increases outward parallel to the wall while continuously decreasing its average flow speed. This results in an increase in the conductive heat flux magnitude as the radial distance increases away from the Nusselt number peak, giving rise to higher thermal stresses in the solid materials (Downs & Landis, 2009). Also, it has a

high potential to increase the local heat transfer rates near the stagnation point for a given coolant mass flow rate (Claretti, 2013). Impingement cooling as a whole has led to improved heat transfer rates of the coolant and blade material, which has helped to improve overall efficiency of the turbine engine. Therefore, it is within the scope of this study that jet impingement cooling be investigated for rocket nozzle applications.

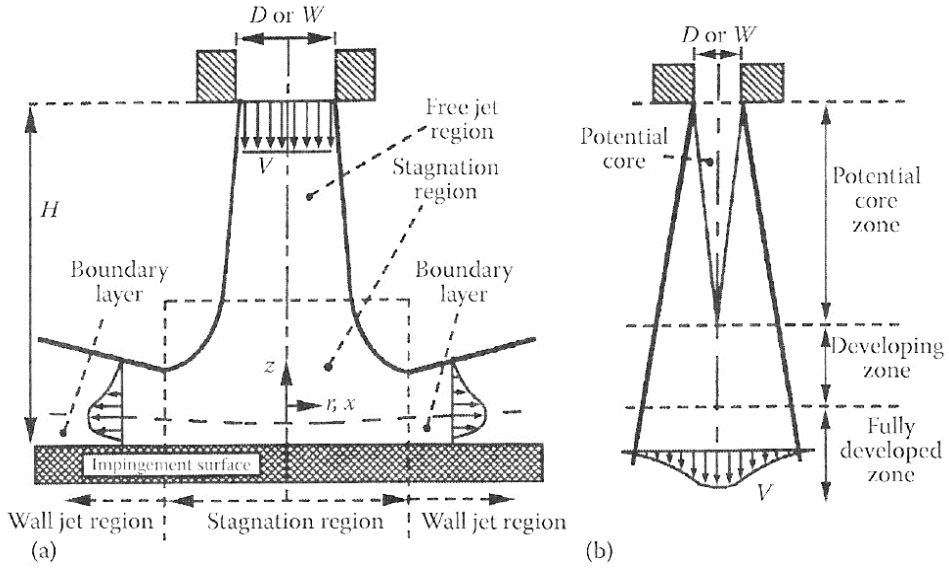

Figure 1.5: Impinging Jet Flow a) region development, b) jet core development (Han *et al.*¸2001)

1.7. Conjugate Heat Transfer

With the desires to improve the efficiency of cooling systems, studies are being done to investigate the benefits of coupling fluid and solid heat transfer analysis. This is for a more accurate model of the surface temperatures. Conjugate heat transfer (CHT) is a heat transfer analysis method which simultaneously incorporates 3-D conduction in solids with the convection in fluids while a heat exchange occurs between the thermally interacting materials (Cukurel *et al.*, 2015). It is a way to assess the multi-dimensional conduction to the convection on the hot gas side within high gradient situations. This is

beneficial when determining the local metal temperatures, which is dependent of the local flow, material thickness (th) and the thermal conductivities (k).

Conjugate heat transfer analysis is often assessed through both experimental testing and computational analysis. It is noted that experimentation has high associated cost, so engine flow conditions are typically scaled for testing purposes (Han *et al.*, 2001). When performing a computational analysis, it is essential to model the accurate flow conditions of a real gas turbine or rocket engine.

1.8. Computational Fluid Dynamics

Computational Fluid Dynamics (CFD) is a 3-D modeling software which provides a more complete physical understanding of the flow field and thermal properties of a system. It provides quantitative predictions while being a visual aid for modeling engine geometries, based on the Navier-Stokes equations, which relates the velocity (v), pressure (P), viscosity (μ) and density (ρ) of a moving fluid (Zuckerman & Lior, 2006). The equations can be rewritten into a simplified form by introducing the rate of strain tensor (S_{ij}), shown by Equations 2 and 3 below (Zikanov, 2010). This is advantageous when designing efficient heat transfer models.

$$\rho \frac{Dv}{Dt} = -\nabla P + \nabla \left[2\mu S_{ij} - \frac{2}{3}\mu(\nabla \cdot V)\delta_{ij} \right] \quad (2)$$

$$with: \quad S_{ij} = \frac{1}{2}\left(\frac{\partial u_i}{\partial x_j} + \frac{\partial u_j}{\partial x_i} \right) \quad (3)$$

1.8.1. Turbulence Modeling

When selecting a turbulence model, both the turbulent transport model itself and wall-treatment model must be carefully considered. This is especially important within heat

transfer studies. The wall treatment is important for accurate near wall predictions of the thermal gradients and flow behavior (Zuckerman & Lior, 2006). It is known that for impingement studies, CFD models will struggle to capture the intricacies within the simulations. The most common practice for engine cooling analysis is to thus use a time-averaged k-epsilon Reynolds-averaged Navier-Stokes (RANS) model. This model uses the Reynolds stress tensor (τ_{ij}) for the total stress tensor by averaging over the Navier-Stokes equations to account for turbulent fluctuations in the fluid's momentum (Zikanov, 2010). Although RANS is a widely used turbulence model, the system can only be solved numerically once the mean τ_{ij} is found for average quantities.

$$\tau_{ij} = 2\mu_{turb}S_{ij} - \frac{2}{3}\rho(TKE)\delta_{ij} \quad (4)$$

It is noted that RANS turbulence results are not completely reliable due to the chaotic nature of turbulent flows. Thus, it is extremely important to have a confident benchmark simulation against well-established and accepted experimental data. Using the two-equation eddy viscosity (μ_{turb}) approach, the k-epsilon model provides a good compromise between robustness, computational cost, and accuracy, while its v^2f model is known to more accurately predict heat transfer rates (Behnia *et al.,* 1997).

1.9. Objectives

The primary objective of this research was to perform a preliminary feasibility study of regenerative cooling utilizing jet impingement onto a SSME-like liquid rocket engine nozzle throat region. It is hypothesized that a combined cooling configuration will help increase the heat transfer rates for a rocket nozzle. Based on the extensive literature review explained in the subsequent chapter, to the best of the author's knowledge, a

regeneratively cooled rocket nozzle has yet to be studied utilizing impingement cooling. The following objectives are therefore studied in this paper:

- Establish correlations from a literary empirical model to use for benchmarking purposes.
- Create a benchmark model for both non-CHT and CHT studies with air to simulate gas turbine cooling.
- Establish modeling methods from the air CHT study.
- Assess a 1-D thermal resistance model for setup validation purposes or various nozzle wall materials, such as Stainless Steel 304, Inconel x-750, copper, and ABS plastic, to determine their feasibility.
- Utilizing STAR-CCM+ CFD software, conduct a 3-D computational investigation of jet impingement cooling applied to a regeneratively cooled rocket nozzle geometry similar to the Space Shuttle Main Engine combustion parameters. Supercritical LH2 is used as the fuel and coolant.
- Assess the lateral conduction effects within the nozzle wall materials through CHT analysis. Investigate the heat transfer rates of rocket CFD simulations to see their resulting CHT effects with the selected materials. Overall, the nozzle wall material integrities are analyzed to ensure that the maximum wall temperature remains below the melting temperature.

2. Literature Review

2.1. Introduction

For liquid propellant rocket engines (LPREs), their high combustion temperatures raise the overall temperature of the rocket and thus a cooling technique must be implemented. In his 1964 report, Coulbert explains the applicable ranges and limitations of rocket engine cooling techniques, and gives insight on how to select the most suitable method for an individual engine. With space propulsion systems themselves displaying a wide range of thrust capabilities and burning times, not all methods are appropriate for every rocket. He proposed that the propulsion requirements, weight analysis, and performance penalties are to be considered. Propellant choice will determine the combustion gas temperature, which is a driving parameter in rocket engine heat transfer analysis. With the wall temperatures needing to be kept relatively low, the heat transfer within the wall is a primary concern for rocket design.

2.2. Regenerative Cooling

Regenerative cooling is a widely used thrust chamber cooling method which pushes high velocity coolant over the hot gas chamber walls to cool the engine. As it exits the cooling chamber, the heat addition it gained during cooling is used as a propellant for the rocket system. The main advantages for using regenerative cooling are its long, continuous run time, negligible heat loss, and light weight structure. Therefore, it is found to be best used for high thrust propulsion engines, such as the SSME (Coulbert, 1964).

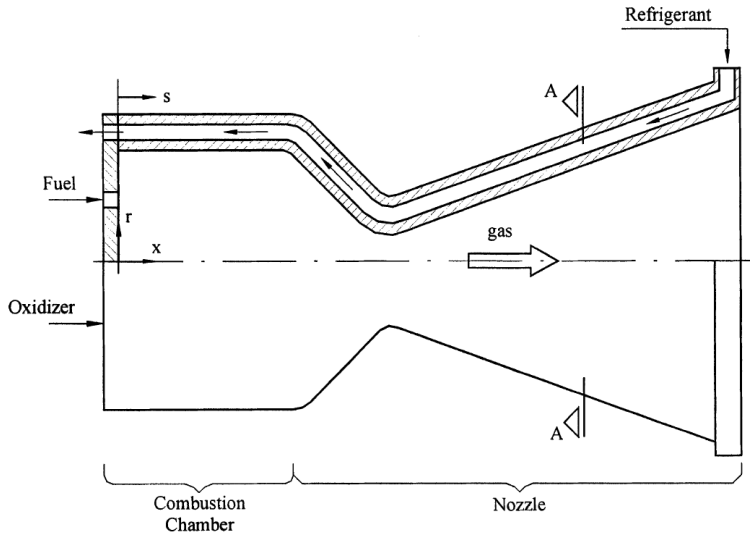

Figure 2.1: LPRE CD Nozzle with Regenerative Cooling (Marchi *et al.*, 2004)

Marchi *et al.* (2004) presented a 1-D mathematical model for predicting engine flow of a regenerative cooling system through a convergent-divergent (CD) nozzle, whose schematic is shown above in Figure 2.1. Monitoring the temperature distribution imposed from the combustion gases along the wall is essential for maintaining structural integrity and prolonging the engine's lifetime. They computed the empirical relationships for the coolant flow and heat conduction through the wall. Additionally, a numerical model with 1-D simplifications was generated where the gas and coolant flows were coupled with the heat conducted through the wall. To demonstrate the model, a hypothetical large LPRE with copper walls and LH2 as its coolant was evaluated.

Kang & Sun (2011) developed and compared multi-dimensional, numerical methods for predicting the hot gas and CFD simulations for coolant side heat transfer rates in a regeneratively cooled rocket engine thrust chamber. They took a conjugate approach for the cryogenic LOX/LH2 nozzle analyzed. Their methodologies were assessed from existing data of high enthalpy, hot-firing tested thrust chambers completed at the Arnold Engineering Development Center in Tennessee. It was concluded that a full analysis

utilizing CHT is most effective when assessing rocket heat transfer.

Miranda & Naraghi (2011) conducted a CFD study which modeled film cooling in the SSME with wall temperatures ranging from 300 to 833 K. They studied multiple cases with varying degrees of fuel and oxidizer mixing. When pure hydrogen is used, maximum film cooling effects are observed compared to a mixture. They found for each case the film cooling effectiveness reduces the wall heat flux and the associated heat transfer coefficient.

Kim *et al.* (2014) carried out a CHT and hydraulics study of a regenerative cooling designed rocket engine with kerosene. A 1-D thermal resistance model based on Nusselt number correlations was implemented into the computational analysis. Once completed, the work was validated to an actual regeneratively cooled double-walled thrust chamber for temperature increase and pressure drop though the cooling passages. The results show good agreement with the numerical results.

Rajagopal (2015) studied the performance of a LOX/LH2 regeneratively cooled engine with a larger than average expansion ratio of about 100:1. The influence of the thermal material properties and wall thickness were shown to have a large impact on the conductive heat transfer. Looking at 3-D simulations for steel and for copper walls, steel proved to better predict the maximum wall temperature. This can be attributed to steel's higher thermal conductivity.

Naraghi *et al.* (2006) investigated the effectiveness of a dual regenerative cooling configuration for LPREs. A conventional, singular regenerative cooling system has one channel where the heated coolant reaches the nozzle exit and is used for engine combustion. However, a dual channel setup allows the coolant to travel in separate directions of the throat. This is advantageous because the overall coolant temperature is lower thus,

providing a higher cooling temperature. This study demonstrated the effectiveness of a dual circuit flow of a SSME-like model within CFD. It was found that the dual circuit design reduces the nozzle throat wall temperatures and gives a lower pressure drop across the wall.

Although there is an extensive amount of regenerative cooling studies completed, most investigations focused on channel flow with an emphasis on the hot gas side heat transfer. More recently, coolant side studies have been conducted with conventional and updated configurations. With the need to cool the rocket engine wall temperatures, particularly at the nozzle throat where the heat load is highest, more innovative techniques must be also studied. Therefore, this study proposes a jet impingement cooling application for a regeneratively cooled rocket nozzle.

2.3. Impingement Cooling

Gas turbine engines require high heat transfer rates so that they may maintain high temperatures and cycle efficiency (Bunker, 2007). Young & Wilcock (2002) widely studied modeling various gas turbine cooling methods and their associated losses. A well-known and widely used turbine cooling technique which they studied is jet impingement cooling. Due to a wide range of applications for impingement cooling, several studies have been completed with varying combinations of geometric and thermodynamic parameters applied. Many papers give in-depth explanations of the various experimental and computational studies, such as those by Martin (1977), Goldstein *et al.* (1986) and Han & Goldstein (2001). They have all contributed comprehensive reviews on heat transfer aspects of impinging flows to include variations in jet-to-target spacing (Z/D), nozzle geometries and jet arrangements. A selection of relevant air impingement literature relevant to this study is discussed throughout the following pages.

Martin (1977) reviewed a collection of experimental work completed by multiple authors of his time who studied general impingement effects. He discusses a thorough analysis of impinging jet heat transfer for various jet configurations including single round or slot nozzles (SRN or SSN) and array round or slot nozzles (ARN or ASN). With these configurations, he was able to take average heat transfer rate values and discuss the relationships between the geometrical ratios, such as the radial distance ratio(r/D) and the jet-to-target plate spacing (Z/D), and their resulting Nusselt numbers (Nu). For this study, a SRN orifice will be implemented.

Claretti (2013) focused his work on the setup and validation of an impingement test with an emphasis on the Nusselt number for the system. An impingement smooth channel flow configuration with the aid of temperature sensitive paint (TSP) is studied for a range of Reynolds numbers from 5,000 to 30,000, streamwise spacing (X/D) of 4, spanwise spacing (Y/D) of 5, and changing jet-to-plate heights (Z/D) of 1, 2, 3, 5, 7, and 9. From his analysis, Claretti concluded, like those before him, that the Nusselt number profile changes as a function of both streamwise location from the stagnation zone and channel height, confirming that as height decreases the heat transfer profile itself will increase, with dependence on the Reynolds number used during his experiments. Many other authors, such as Hylton *et al.* (1983), Dees (2010), and Lee *et al.* (2014), have also concluded that the Nusselt numbers for jet impingement show a strong dependence on the impinging jet Reynolds number (Re_{jet}). Their work will be discussed in detail later in this chapter.

Brown *et al.* (1968) studied the heat transfer characteristics of the leading edge region of a gas turbine blade. The experimental impingement system allowed the acquisition of heat transfer data in a cold flow and full-size model. The basic

considerations, experimental apparatus and procedure, data analysis and stagnation Nusselt number results were discussed. They found that when the impingement geometry and location were held fixed and only Re is varied, Nu will vary by Re to a power and the slope of the stagnation Nu versus Re is nearly the same for all Z/D values.

Florschuetz *et al.* (1981) were one of the first researchers who investigated the heat transfer characteristics of jet array impingement, focusing on the effects of the initial crossflow along a flat plate. An extensive study of several in-line staggered impingement arrays was conducted for an average jet Re of 5,000 for 10 spanwise jet holes. Spacing was set to X/D of 4 to 8, Y/D of 5 to 15, and Z/D from 1 to 3. They produced a simple analytical model of the channel flow field, which is still widely used today to calculate the Re of each impinging jet in an array. An empirical correlation given in Equation 5 for Nu with respect to the test section's geometric parameters A, B, m, and n was established. G_c/G_j is representative of the ratio of the 1-D mass flux models.

$$Nu = A * Re_j^m * 1 - B\left[\left(\frac{Z}{D}\right) * \left(\frac{G_c}{G_j}\right)^n\right] * Pr^{1/3} \quad (5)$$

Al-Hadhrami *et al.* (2011) studied the heat transfer effects on three channel height ratios (Z/D) of 5, 7, and 9 with a Reynolds number of 18,800 for given outflow orientations of an inclined heated copper plate. They investigated three different orifice jet plate impingement configurations for centered, staggered, and tangentially placed holes. They found that a plate with centered holes gives better heat transfer rates compared to the other configurations, with the highest Nusselt number resulting from the higher Z/D of 9.

2.3.1. Conjugate Heat Transfer Studies

Although a substantial number of literature has been written about impingement cooling, there remains a limited number of studies to include both the fluid and solid heat transfer rates. More recently there has been an increase of research to include a CHT study to help to fully understand the phenomenon occurring within the entire system to help predict the surface temperatures.

Hylton *et al.* (1983 documented an early CHT study whose work pioneered CHT experiments for future turbine applications. From the computational benchmark created, the work focused on non-film cooled metal vanes and its heat transfer distribution within a 2-D flow field, matching against the Mark II and C3X airfoils. The metal vanes were cooled via cooling channels along the external surface at an airfoil's midspan using surface thermocouples to gather the temperature data. The data obtained from their experiments, which include internal heat transfer coefficient, external surface temperature distribution, and heat flux, were used to solve the conduction equations. This study showed that the overall heat transfer rate is strongly dependent on the Reynolds number value. This work is widely used as a benchmark for proceeding optimization studies for blade channel cooling.

Dees (2010) experimental work is the first matched Biot number (Bi) model experiment where he conducted a study for a scaled up, adiabatic simulated turbine vane. The Biot number measures the temperature drop in a solid relative to the temperature difference between a solid and fluid. He provided detailed measurements on and around the scaled up conducting airfoils with and without film cooling. Dees also found that along the jet centerline, thermal boundary layer effects are less influential due to the development

of a new, thin boundary layer. The results showed that the external surface temperatures are highly dependent on the external and internal heat transfer coefficients.

Lee *et al.* (2014) discussed the array impingement effects of jet-to-target plate distances and Reynolds numbers on the heat transfer of a flat plate, with Reynolds number ranging from 8,200 to 52,000 for Z/D from 1.5 to 8 and a constant X/D and Y/D of 8. They concluded that different jet-to-target distances result in different interactions due to the altered vortex flow fields. It is observed that the local and spatially-averaged Nu show a strong dependence on Re, and that lower overall Nu values occur at very high Z/D heights.

Mensch & Thole (2014) conducted a CHT analysis via experiments and computational simulations to study both external and internal cooling techniques. They investigated the overall effectiveness on the impingement channel height for a turbine blade endwall, with a focus on the influence of the internal impingement cooling due to variations in the geometry on the wall temperatures and internal heat transfer coefficients. They then built upon the results for a blade endwall with impingement cooling. Initially a jet array configuration of 28 impinging holes was set up and then investigated for its effects with 10 cylindrical film cooling holes angled at 30°. They also incorporated a matched Biot number study to the work. It was found that the overall effectiveness decreased at the center of the impingement area, with a larger Z/D being able to cool a wider area of the endwall.

Vynnycky *et al.* (1998) analyzed the mathematical model for the forced convective heat transfer and solved the 2-D CHT problem for a rectangular thermally conducting slab within the thermal and viscous boundary layers. They numerically solved the momentum and heat transfer equations using a finite-difference method and included the effects of Reynolds number (Re), Prandtl number (Pr), thermal conductivity (k) and aspect ratio

between the slab and fluid taken into consideration.

Curkurel *et al.* (2015) investigated the CHT conduction-convection coupling effects of a jet impingement by steady state and transient (unsteady) analysis with an infrared thermography method capturing the heat transfer coefficients. Looking at various materials, such as steel, copper and Inconel, the solid thermal conductivities (k) and Biot number variations are found for Reynolds number of 34,000 and 37,000. They concluded that this transient method, when temperature changes as a function of time, was comparable to Nu accuracy and effectiveness as that of a steady method. The average heat transfer varied by up to 9% depending on the material, with copper and Inconel showing the lowest and highest values respectively.

2.3.2. Computational Fluid Dynamic Studies of Jet Impingement

Rahman *et al.* (2000) were the first to numerically model CHT process where heat was transmitted through a solid body from a heat source located on one side and fluid impinging on the opposite side for high Prandtl number fluids. They conducted a CHT experiment for a free jet applicable in the stagnation zone. Using CFD, they computed the results of the velocity, temperatures, pressures, local and average heat transfer coefficients along with the fluid flow distribution. It was found that at large Reynolds number, the fluid becomes more complicated from the possibility of flow separation at the blade's leading edge. There is subsequent reattachment and recovery of the laminar boundary layer from this flow.

Zuckerman and Lior (2006) analyzed the numerical modeling of impingement heat transfer while tabulating the comparisons for different CFD turbulence models with the anticipation of the Nusselt number error within impingement jet heat transfer. The k-

epsilon, k-omega, Reynolds stress model, algebraic stress models, shear stress transport, and v^2f turbulence models were investigated with their results given in Table 2.1. They discussed the differences between DNS, LES and RANS models used to aid impingement experiments and the trends commonly seen in CFD studies. CFD is widely used today within industry for its increased efficiency of numerical modeling predictions, sensitivity analysis and device designing.

Table 2.1: Comparisons of CFD Turbulence Models for Impingement Cooling (Zuckerman & Lior, 2007)

COMPARISON OF CFD TURBULENCE MODELS USED IMPINGING JET PROBLEMS

Turbulence model	Computational cost (time required)	Impinging jet transfer coefficient prediction	Ability to predict secondary peak
k–ε	★★★★ Low cost	★ Poor: *Nu* errors of 15–60%	★ Poor
k–ω	★★★★ Low–moderate	★★ Poor–fair: anticipate *Nu* errors of at least 10–30%	★★ Fair: may have incorrect location or magnitude
Realizable k–ε and other k–ε variations	★★★★ Low	★★ Poor–fair: expect *Nu* errors of at 15–30%	★★ Poor–fair: may have incorrect location or magnitude
Algebraic stress model	★★★★ Low	★★ Poor–fair: anticipate *Nu* errors of at least 10–30%	★ Poor
Reynolds stress model (full SMC)	★★ Moderate–high	★ Poor: anticipate *Nu* errors of 25–100%	★★ Fair: may have incorrect location or magnitude
Shear stress transport (SST), hybrid method	★★★ Low–moderate	★★★ Good: typical Nu_0 errors of 20–40%	★★ Fair
v^2f	★★★ Moderate	★★★★ Excellent: anticipate *Nu* errors of 2–30%	★★★★ Excellent
DNS/LES time-variant models	★ Extremely high (DNS available for low *Re* only)	★★★★ Good–excellent	★★★★ Good–excellent

[★ indicating undesirable model characteristics, to ★★★★ indicating excellent model characteristics.]

Zuckerman & Lior concluded that the v^2f model will give the best prediction of a secondary Nusselt number peak. The percent error values per turbulence model in relation

to Nusselt number is tabulated in Table 2.2. Zuckerman and Lior (2007) then proceeded with additional computational work for ASN impingement at a Reynolds number range of 5,000 to 80,000 using the v^2f turbulence model from their previous conclusions. The number of nozzles varied from 2 to 8, with target diameter size from 5 to 10 times the hydraulic diameter (D). They concluded that when seeking to increase the Nu, the Reynolds number effects will dominate.

Table 2.2: CFD Modeling Errors for SRN Impingement onto a Flat Plate (Zuckerman & Lior, 2007)

Model	% error in Nu in stagnation region	Max. % error in Nu in wall jet, $2 < r/D < 5$	Max. % error in Nu in wall jet, $r/D \geq 5$
SST	+50	−25	−31
v^2f	+30	−5 to +5	−22
Realizable k–ε	+22	−19 to +6	+30
Standard k–ε	+22	−40	−53
RSM	+16	−40	−40

Behnia *et al.* (1997) discussed that to properly understand the heat transfer process for jet impingement, the flow, geometry, and turbulence must also be well understood. Without a full understanding, comparisons between experimental and computational work may not be accurately related. They utilized the v^2f turbulence model for its known success for predicting heat transfer rates.

Many authors, such as O'Donovan & Murray (2007), have reported witnessing secondary peaks in the heat transfer distribution of an impinging jet. They observed that in some cases, two radial peaks are observed. The thickening of the wall boundary layer moving radially outwards from the stagnation point will decrease the heat transfer rate. However, when the flow transitions to fully turbulent, the heat transfer peak increases to a secondary peak. This additional peak, even at large Z/D, is created as a result of wall jet remaining influenced by the flow of the impinging jet beyond its potential core region. The

secondary maxima occurs at about 2 jet diameters from the stagnation point as a result of entrained air caused by vortex rings in the shear layer.

Buchlin (2011) carried out experimental and computational studies for SRN, SSN, ARN and ASN configurations to analyze the flow and geometric parameters of the impingement while investigating an isothermal round jet impinging perpendicularly onto a flat plate, an axisymmetric thermal field was observed. The resulting concentric hot and cold rings in the thermal scene displays the presence of high and low heat transfer regions. These rings play an important role within understanding the connections between the heat transfer and flow distributions.

2.4. Empirical Model: Martin (1977)

From the literature, the importance of the correlations between the Nusselt number and the impingement jet-to-target-plate spacing (Z/D) of the setup is observed. Holger Martin (1977) studied general impingement effects for various jet configuration values and discussed the relationships between the geometrical ratios and their resulting Nusselt numbers. Looking at SRN impingement, Martin took the heat transfer measurements of Schlunder and Gnielinksi (1967), Gardon and Cobonpue (1962), Petzold (1964), Brdlick and Savin (1965) and Smirnov *et al.* (1961) to create the following empirical correlation equation.

$$\left(\frac{\overline{Sh}_1}{Sc^{0.42}}\right)_{SRN} = \left(\frac{\overline{Nu}}{Pr^{0.42}}\right)_{SRN} = \frac{D}{r}\left(\frac{1-1.1\frac{D}{r}}{1+0.1\left(\frac{Z}{D}-6\right)\frac{D}{r}}\right) F(Re) \tag{6}$$

$$with: \quad F(Re) = 2Re^{0.5}\left(1+\frac{Re^{0.55}}{200}\right)^{0.5} \tag{7}$$

This relationship uses F(Re) defined for a smooth curve expression so that the discontinuities of the functional variation at the limits of the Reynolds number ranges are

avoided. The correlation is valid for ranges:

$$2{,}000 \leq \mathrm{Re} \leq 400{,}000$$

$$2.5 \leq \mathrm{r/D} \leq 7.5$$

$$2 \leq \mathrm{Z/D} \leq 12$$

If analyzing between the stagnation point up to r/D of 2.5 and a Z/D value other than 7.5, a correction function $k\left(7.5, \frac{r}{D}\right) \equiv 1$ must be utilized to properly use the corresponding log scale data plot for the ratio of the average Nusselt number (Nu) to Prandtl number (Pr) raised to 0.42, $\frac{\overline{Nu}}{Pr^{0.42}}$ versus the jet Reynolds ($\mathrm{Re_{jet}}$), shown in Figure 2.2. The exponent 0.42 for Prandtl number is determined from its comparison between the mass transfer measurements with the heat transfer data for air, which has a known Pr value of 0.7. Note that Nu= Nu (Re, Pr, r/D, Z/D) is of the average value, not the local value. This requires an average heat transfer coefficient within its calculations. The logarithmic scaled plot below shows that as r/D increases, Nu will monotonically decrease for all ranges of Re.

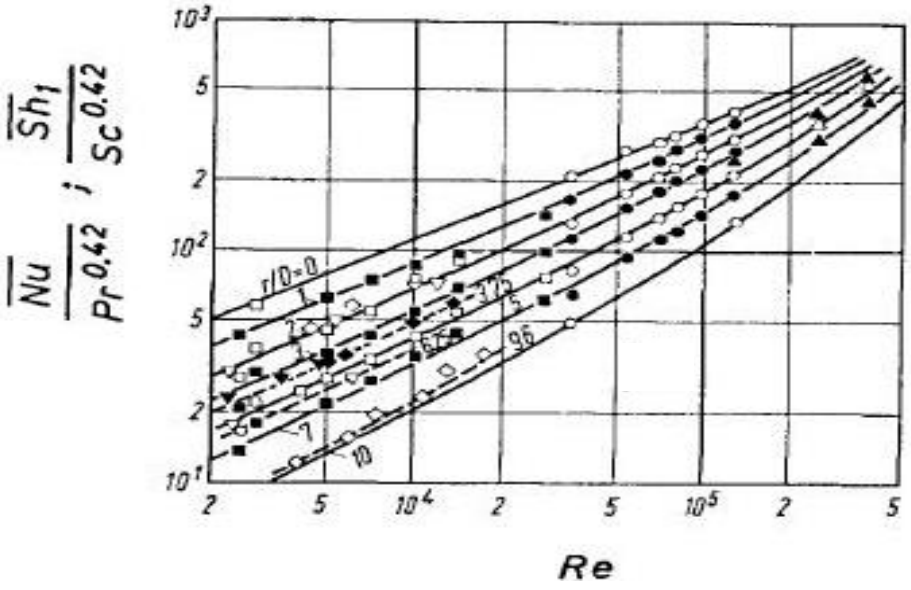

Figure 2.2: Heat and Mass Transfer for Impinging Flow of SRN at Z/D = 7.5 (Martin, 1977)

3. Data Reduction

3.1. Introduction to Heat Transfer Analysis

Proper heat transfer analysis is required for the design, testing, and validation of an engine. Within heat transfer there are three main modes: convection, conduction, and radiation. For this study, convection and conduction are utilized, and all radiation effects are ignored. Convection is used to describe the energy transfer between a surface and fluid moving over the surface, and conduction is the energy transfer within a medium due to a temperature gradient (Bergman & DeWitt, 2011).

3.1.1. Fluid Flow Analysis

When analyzing the flow for any fluid, the dominating characteristic is the jet Reynolds number. The Reynolds number (Re) is a dimensionless ratio of the momentum forces to viscous forces of a fluid, used to determine if the flow is laminar, turbulent, or transitioning. It assesses the fluid's density (ρ), velocity (v) and characteristic length compared to its dynamic viscosity (μ) at the nozzle exit. The dynamic viscosity quantitatively measures the forces needed to overcome the internal friction occurring within the flow. Within impingement studies, it is common practice to use the nozzle diameter (D) as the characteristic length within fluid calculations. The Reynolds number equation with D is shown below.

$$Re = \frac{\rho v D}{\mu} \tag{8}$$

In addition to the Reynolds number, the mass flow rate ($\dot{m}$) of the fluid can also be found. This is an important quantity to help gauge how much fluid is passing through the domain for any given instance in time.

$$\dot{m} = \rho v A \tag{9}$$

Analyzing for a steady state method, the heat transfer rates and hot side temperature must reach thermal equilibrium independent of time. This helps the solution to converge at a faster rate, leading to overall simpler solutions with less computing time and cost savings. The higher the Reynolds number, the shorter amount of time is required for a flow to reach steady state conditions (Sutton, 2000). This is due to the higher velocity of the fluid which helps to enhance the convective heat transfer process.

The Prandtl number (Pr) is another important ratio for fluid flow analysis. It compares the viscous to thermal boundary layer of the fluid, relating its dynamic viscosity (μ) and specific heat (c_p) to the thermal conductivity (k). For jet impingement, the Pr is used to accurately predict the average heat transfer coefficient. A typical Pr value for air is 0.7, but for other gases or liquids, the Pr number is represented as,

$$\text{Pr} = \frac{\mu * c_p}{k} \tag{10}$$

3.2. Heat Transfer Modes

3.2.1. Convective Heat Transfer

Convection heat transfer is described by Newton's Law of Cooling, which states that the rate of heat loss from a body is proportional to the temperature difference between the body and its surroundings as given by the following equation. Here, Q_{conv} is the heat transfer rate, h is the convective heat transfer coefficient, and A is the surface area.

$$Q_{conv} = hA(\Delta T) \tag{11}$$

Dividing Equation 11 by its unit area, the convective heat flux (q''_{conv}) is obtained, as shown in Equation 12.

$$q"_{conv} = h(\Delta T) \tag{12}$$

For these equations, the temperature difference is the difference between the surface temperature, the adiabatic wall (T_{aw}), and the reference temperature. For impingement studies, the reference temperature is the impinging jet temperature (T_{jet}). From Equation 12, h can be obtained as,

$$h = \frac{q"}{\Delta T} \tag{13}$$

Equating the heat transfer coefficient (h) with the fluid's thermal conductivity (k_{fluid}) and the jet diameter (D_{jet}), the Nusselt number (Nu) is found by Equation 14. Nusselt number by definition is the ratio of convective to resistance across the boundary of interest (Bergman & De Witt, 2011). The convective thermal resistance for use in the 1-D analysis is the inverse of Equation 13.

$$Nu = \frac{h*D}{k_{fluid}} \tag{14}$$

$$R_{conv} = \frac{\Delta T}{q"} = \frac{1}{h} \tag{15}$$

For conventional turbulent fluid flows in a smooth pipe, the Nu is expressed by the Dittus-Boelter Correlation. The exponents, m and n, can be taken as 0.8 and 0.3 respectively. The n exponent value depends on if the heating or cooling of a turbulent flow. The constant coefficient, C, has been seen in literature to range from 0.21 to 0.33 resulting from experimental tests depending on the turbulence characteristics (Moran & Shapiro, 2011).

$$Nu = C * Re^m * Pr^n \tag{16}$$

Hot Gas Side Heat Transfer in Rocket Nozzles

Within a rocket nozzle, the combustion chamber design parameters have a major impact on the overall propulsive power and heat transfer rates of the system. Particularly for the hot gas side, combustion temperatures can reach upwards of 3600 K (Turner, 2010). This value depends on the propellants used and the operating conditions of the engine. To monitor the heat transfer rates on the hot combustion side, the adiabatic wall temperature (T_{aw}) and heat transfer coefficient (h) must be found.

The adiabatic wall temperature of the combustion gas is dependent of the chamber temperature (T_{ch}), Mach number (M), Prandtl number (Pr) and specific heat ratio (γ). A local recovery factor (rf), which represents the ratio of the frictional temperature increase to the adiabatic compression increase, is utilized and defined as $Pr^{0.33}$ for turbulent flows. The effective recovery factor (Rf) typically varies from 0.9 to 0.98 (Huzel & Huang, 1992).

$$T_{aw} = T_{ch} * Rf \tag{17}$$

$$with: \quad Rf = \left[\frac{1+rf\left(\frac{\gamma-1}{2}\right)M^2}{1+\left(\frac{\gamma-1}{2}\right)M^2}\right] \tag{18}$$

Although conventional turbulent boundary layer correlations have been developed as seen above in Equation 16, an accurate approximation of the heat transfer coefficients in rocket nozzles was developed by Bartz (1957). The well-known correlation for the hot gas side convective heat transfer coefficient (h_g) equation uses constants C of 0.026 and ω of 0.6.

$$h_g = \left[\frac{C}{D_*^{0.2}}\left(\frac{\mu^{0.2}c_p}{Pr^{0.6}}\right)_0\left(\frac{P_{ch}g}{C^*}\right)^{0.8}\left(\frac{D_*}{r_c}\right)^{0.1}\right]\left(\frac{A_*}{A}\right)^{0.9}\sigma \tag{19}$$

$$with: \quad \sigma = \frac{1}{\left[\frac{1}{2}\frac{T_{wall}}{T_o}\left(1+\frac{\gamma-1}{2}M^2\right)+\frac{1}{2}\right]^{0.8-(\omega/5)}\left[1+\frac{\gamma-1}{2}M^2\right]^{\omega/5}} \tag{20}$$

This equation is dependent on the flow parameters, such as the fluid's dynamic

viscosity (μ), specific heat (c_p), Prandtl number (Pr) and chamber pressure (P_{ch}). Geometrical parameters dependent on the nozzle shape and size, such as throat diameter (D*), radius of curvature (r_c) and respective areas (A, A*), are also taken into consideration. It is noted that the expression within the brackets is constant throughout combustion calculations. Factor σ incorporates the boundary layer property variation parameters.

From this equation, it is also noted that for a small throat diameter a larger heat flux will be later produced, with maximum heat flux occurring at the nozzle throat (Huzel & Huang, 1992). This further demonstrates that as we continue to push nozzle performance limits, better heat transfer rates we can be developed and utilized for increased rocket engine thrust performance.

3.2.2. Conduction Heat Transfer

Conduction heat transfer is governed by Fourier's Law, which implies that the heat flux through a solid surface is a directional quantity normal to the cross-sectional area (Bergman & DeWitt, 2011). Similarly to convection, Q is the heat transfer rate. When divided by the area, the conductive heat flux ($q"_{cond}$) is obtained. Within these equations, k is the thermal conductivity of the solid.

$$Q_{cond} = kA\frac{\Delta T}{L} \tag{21}$$

$$q"_{cond} = k\frac{\Delta T}{L} = k\frac{\Delta T}{th} \tag{22}$$

The conductive thermal resistance show in Equation 23 is the inverse of the above equation excluding the temperature gradient in its calculation.

$$R_{cond} = \frac{th}{k} \tag{23}$$

For solid materials, the Biot number (Bi) allows conduction problems to include

surface convective effects. The Bi number quantifies the temperature drop in a solid with respect to the temperature difference between the solid surface and fluid (Berman & DeWitt, 2011). It represents the ratio of conduction and convection thermal resistances, using a thermal conductivity (k) of a material and the convective heat transfer coefficient (h) to describe the heat transfer from the surface to the adjacent fluid. Within this impingement study, the characteristic length is again given as the jet diameter (D_{jet}).

$$Bi = \frac{h * D_{jet}}{k_{solid}} \tag{24}$$

3.3. Thermal Resistance Modeling

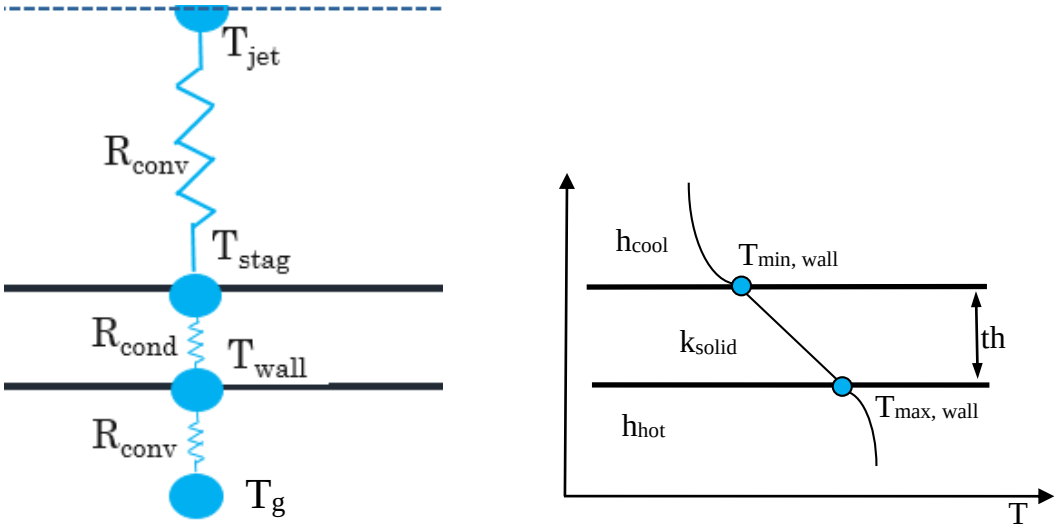

a) b)

Figure 3.1: Thermal Resistance Model of Impingement Jet Setup

When studying the heat transfer effects on an impinging jet, a 1-D flow model, analogous to electrical resistance models, can be analyzed for validation purposes. However, when using the 1-D approximations, the lateral conduction effects within a material are not captured. Therefore, for actual applications a conjugate analysis will be

studied to analyze these effects. As displayed by Figure 3.1a, the heat transfer modes present in this study are conduction and convection. Viewing from the bottom up, the heat flow by convection causes a temperature decrease from the hot gas to the wall. This is then followed by a conductive linear decrease through the wall material, and finally a convective decrease through the coolant boundary layer (Humble, 1995). This particular pattern of heat transfer is shown in Figure 3.1b by a graphical representation of the temperature decrease as a result of this process.

4. Benchmark Model

4.1. Introduction

Within this study, STAR-CCM+ (CD-adapco, Ver. 9.06.011) CFD software was utilized. The computational model created was based on values extracted from data collected by Martin (1977), introduced in Section 2.4, comparable to Martin's experimental work for a perpendicular, turbulent SRN jet impinging onto a flat plate. An initial study was completed for gas turbine cooling, which will then applied to a rocket nozzle geometry. For gas turbine engines, the air jet Reynolds number is typically of the order of 50,000 (Han *et al.*, 2001). Therefore, the model in this study was studied with a Z/D of 7.5 at a Reynolds number of about 50,000.

4.2. Non-CHT Study

Heat transfer predictions were first investigated for a solely fluid air domain so that a confident benchmarking model case could be developed for a fluid and solid domain region later in this study.

4.2.1. Computational Domain & Modeling

Referencing Martin's work (1977), a SRN model with a height spacing (Z) of 127 mm and jet diameter (D_{jet}) of 17 mm was created within STAR-CCM+. These values allowed the model to reach a 7.5 ratio fit for later data comparisons. To assess a range of radial distances outwards from the stagnation point, streamwise (X) and spanwise (Y) distances are each measured to r/D of 9.

Due to the symmetrical feature of an SRN jet, two symmetry planes were added to the two middle portions about the center of the hydraulic jet. This created a quarter scaled

model to save on computational time and cost throughout the analysis. A full 360 degree simulation was completed to ensure symmetry validation, which was conclusive and thus the quarter domain model was further studied.

The quarter jet computational domain is shown in Figure 4.1. A constant thermal boundary heat flux value of 1600 W/m^2, collected from corresponding temperature gradient correlations, was applied to the bottom of the fluid region to simulate a heated wall. Two symmetric planes on the inner two surfaces and outlets of zero gauge pressure on the remaining sides were added. In the present computation, the inlet velocity of the jet was assumed to be uniform and moving purely downward.

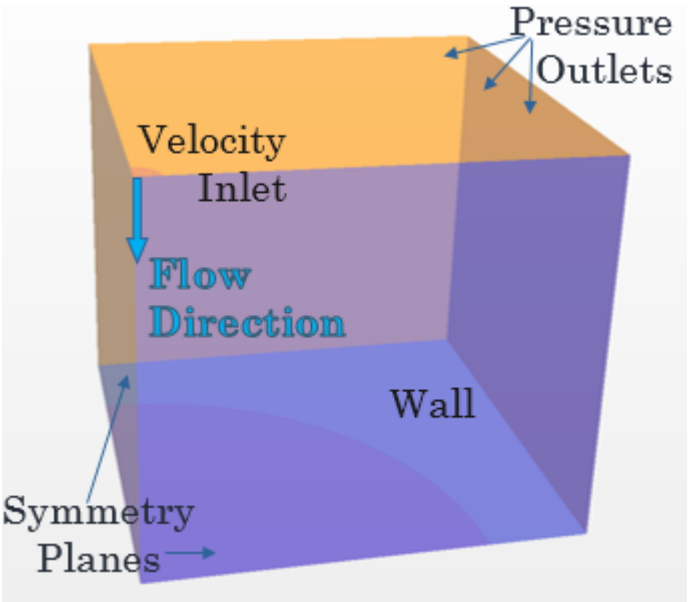

Figure 4.1: Fluid Computational Domain Setup

The heat transfer coefficients (h) were calculated with the jet temperature as the reference temperature for this analysis. The Reynolds number was calculated with an inlet jet velocity of 46 m/s, a hydraulic jet diameter (D_{jet}) of 17 mm, and local fluid properties. First assessing for an air jet of known density (ρ) of 1.16 kg/m^3 and dynamic viscosity (μ) of 1.86E-5 Pa*s, the Reynolds number was calculated using Equation 8 to be exactly

48,361.

4.2.2. Meshing

A meshed model of the fluid region described above is shown in Figure 4.2. A polyhedral mesh model with an average cell size of 5mm was applied throughout the fluid domain. A finer mesh of 0.03D, relative to the jet diameter, all along the heated bottom surface and fluid flow region was used. This was to ensure accurate resolution of the high temperature and velocity gradients near the wall and stagnation point.

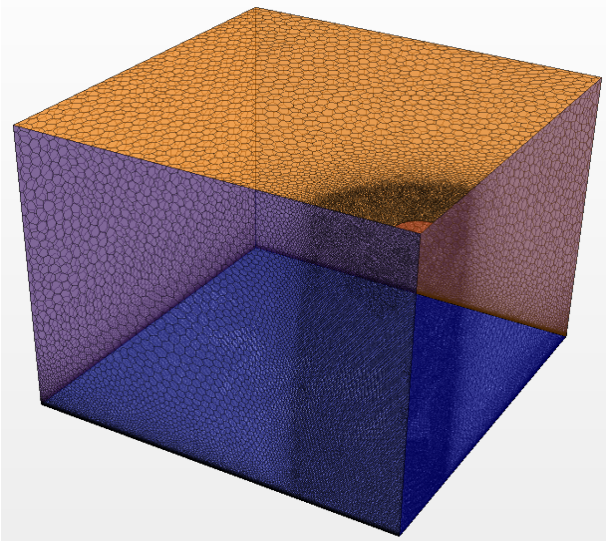

Figure 4.2: Meshed Model for Fluid Domain

It is important for the thermal gradients along the walls to be accurately measured. Boundary layer cells adjacent to the wall allows the wall flow to be calculated more accurately by better predicting the velocity and temperature gradients at those locations by resolving the viscous sublayer. To better resolve the velocity gradients near the wall, 20 boundary layer cells of 1.8 mm overall thickness with a surface growth rate of 1.1 were added from the bottom wall surface, show in Figure 4.3.

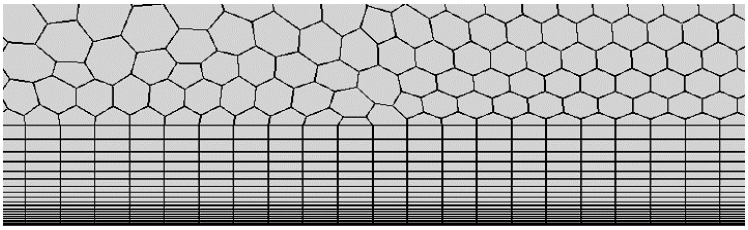

Figure 4.3: Boundary Layers from Wall Surface

Additionally, all y-plus wall treatments were also added to the model. Wall y+ is the non-dimensional wall distance for a bounded flow used to help capture the near wall resolution within a boundary's sublayer (Zikanov, 2010). As stated by researchers such as Zuckerman & Lior (2006), an average wall y+ less than 5 is desirable in the viscous sublayer convective heat transfer simulations. For this fluid domain, a maximum wall y-plus value of 1.71 was obtained, displayed in Figure 4.4.

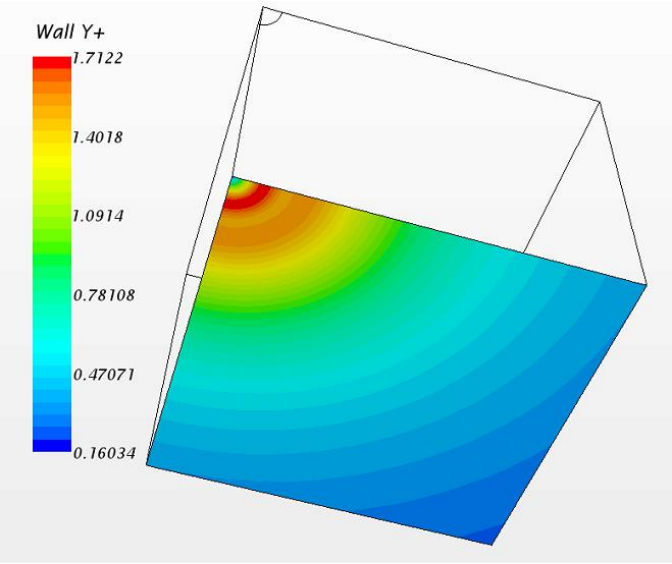

Figure 4.4: Wall Y-Plus Contour

Mesh Independence Study

A mesh independence study was completed using different cell sizes. This portion of the study aids to find the most efficient cell size without a high computational time. Assessing for v^2f simulations, average cell sizes of 10 mm, 5 mm, and 4.5 mm were tested for surface average temperature comparisons along the heated surface. Comparing the 3 sizes, the smallest difference occurred between 5 mm and 4.5 mm with only 0.02% for the temperature for the respective 5.3 million and 8.3 million cells. Therefore, a 5 mm initial base size proved to be efficient for analysis without the added time required with a finer mesh. The final non-CHT cell count totaled to 5.3 million cells. The mesh independence study is graphed in Figure 4.5.

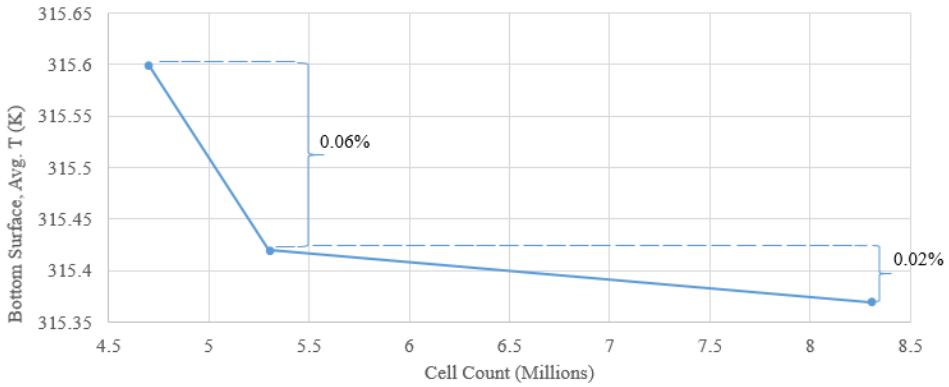

Figure 4.5: Mesh Independence Study

4.2.3. Turbulence Model Testing

Simulations were run for a 3-D, turbulent, steady ideal gas computational study. However, difficulties can arise when numerically modeling impingement cooling within CFD. To resolve these difficulties, a scope of turbulence models were investigated. Utilizing a segregated flow solver, the equations of momentum, mass, and energy were independently solved. Joining the segregated flow with a segregated fluid temperature and

all y+ wall treatments, various turbulence models were then tested to see how quickly they would converge while maintaining sensible heat transfer rate predictions. Throughout the literature it has been noticed that the Reynolds-averaged Navier-Stokes (RANS) models compared to Large Eddy Simulations (LES) will most accurately predict the presence of unsteadiness within turbulent flow (Zuckerman & Lior, 2006). Therefore, variations of the k-epsilon turbulence models were chosen and compared.

For turbulent flow, the k-epsilon models calculate the Reynolds stresses as a function of the flow behavior and the velocity gradients. Using the two-equation eddy viscosity approach, the k-epsilon model provides a good compromise between robustness, computational cost, and accuracy (Behnia *et al.*, 1997). The Realizable Kinetic Energy (Rkε) model is a two equation model solving RANS for the kinetic energy and dissipation (ε) rates. The Elliptic-Blending Kinetic Energy (EBkε) model is more robust and gives better predictions of the near wall effects compared to the Rkε model. The 'normal velocity relaxation model' (v^2f) model includes two additional equations for the normal turbulent stress function (v^2) and the elliptical function. These help to predict the effects of the wall turbulence which is crucial for accurate heat transfer predictions (Zuckerman & Lior, 2006).

Convergence criteria was set to 10^{-11} for all simulations to establish confidence in the results obtained. It was found that RKε took the longest amount of time for the simulation to converge and was inefficient for calculation time purposes. The EBkε model showed improved rates, but still took longer to converge with the same heat transfer results as the v^2f model. As noted by Zuckerman and Lior (2006), the v^2f has the advantage of keeping an eddy viscosity to increase flow stability right up to the solid wall, which avoids

some of the computational stability issues commonly seen. Although it does require a moderate computational cost, its ability to more accurately predict impinging jet transfer to within ±30% error at the stagnation region outweighs the cost (Zuckerman & Lior, 2007). Additionally, it has been known to give the best prediction of a secondary Nusselt number peak (Behnia *et al.*, 1997). Therefore, with its increased abilities and shorter convergence time, a v^2f turbulence model was chosen for the remaining computational analyses.

4.2.4. Results

The heat transfer data collected from the air fluid domain CFD simulation was compared to the literature benchmark model set forth by Martin (1977). A data extraction program, WebPlotDigitizer (Rohatgi, 2015), was used to find the $\frac{\overline{Nu}}{Pr^{0.42}}$ value from the logarithmic Figure 2.2 (Martin, 1977). The average Nusselt numbers at a Reynolds number of 48,361 for r/D of 0, 1, 3, 5 and 7 are found. This range of r/D was chosen for a complete analysis of the wall jet region fluid flow and temperature distribution along the target wall for benchmarking purposes.

Analyzing the air model, a known Prandtl number value of 0.7 is used to back calculate the Nu value from the plot. The resulting CFD Nusselt numbers are gathered and are displayed in Figure 4.6 with respect to their r/D locations. Martin's data (1977) is given with a 20% uncertainty.

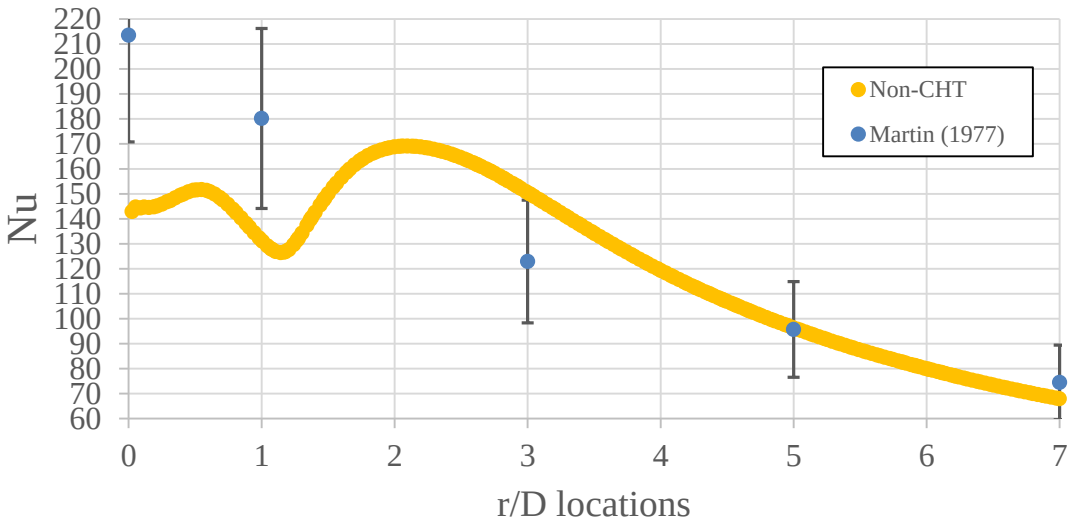

Figure 4.6: Heat Transfer Plot: r/D vs. Nu for Non-CHT case

Martin (1977), shows that as r/D increases for a given Reynolds number its corresponding Nu value will decrease. However, the CFD results obtained show two radial peaks before continuously decreasing. Table 4.1 shows the values and percent differences between the fluid CFD simulation results and Martin's (1977) SRN testing results.

Table 4.1: Nusselt Number Values at Re= 48,361 for Non-CHT case

r/D location	Nu, Martin (1977)	Nu, Non-CHT CFD	% Differences
0 Stagnation Pont	213.5	142.9	33%
1	180.2	130.9	27%
3	122.9	150.1	22%
5	95.7	96.4	0.7%
7	74.5	68.2	8%

4.2.5. Analysis

There are differences between the current study's results and those of Martin (1977). Most noticeable is the 33% under prediction occurring at the stagnation point. This is assumed to be due to poor relaminarization by the CFD to the imposition of the turbulence model taking place at the stagnation point. For r/D values between 0 and 2.2, the location up to the secondary peak, CFD again under predicts the Nusselt number values.

Analyzing the resulting computational Nusselt numbers as a function of the radial distance away from the stagnation point, two distinct peaks are observed. As stated by O'Donovan & Murray (2007), two radial peaks are sometimes seen, with a peak at about 2 diameters from the stagnation point. For this simulation, an initial peak occurs within the stagnation region extending to 1.2 diameters along the solid surface, up to 0.02 meters, and a secondary peak occurring at around 2.2 diameters, at 0.037 meters. As r/D approaches 3, the trend continuously decreases with increased distance which better correlates to data extracted from Figure 2.2.

Looking at the resulting contour images and plots, foremost there is a noticeable temperature fluctuation as r/D increases from the stagnation point. Buchlin (2011), showed that for a SRN impinging jet perpendicular to a flat plate, there is an axisymmetric thermal field which exhibits concentric hot and cold rings radially away from the stagnation region. These rings show that there are high and low heat transfer regions occurring throughout the flow field (Buchlin, 2011). This phenomenon is similarly observed in the current CFD simulations. A visual comparison between the resulting CFD temperature contour and Buchlin's work (2011) is presented in Figure 4.7. This occurrence further shows a relation to the acceleration and reattachment turbulent zones along the solid wall. The non-uniform

temperature field profile matches the varying cold and hot rings radially moving outward from the stagnation zone. The hot temperature rings coincide with the locations of the heat transfer peaks.

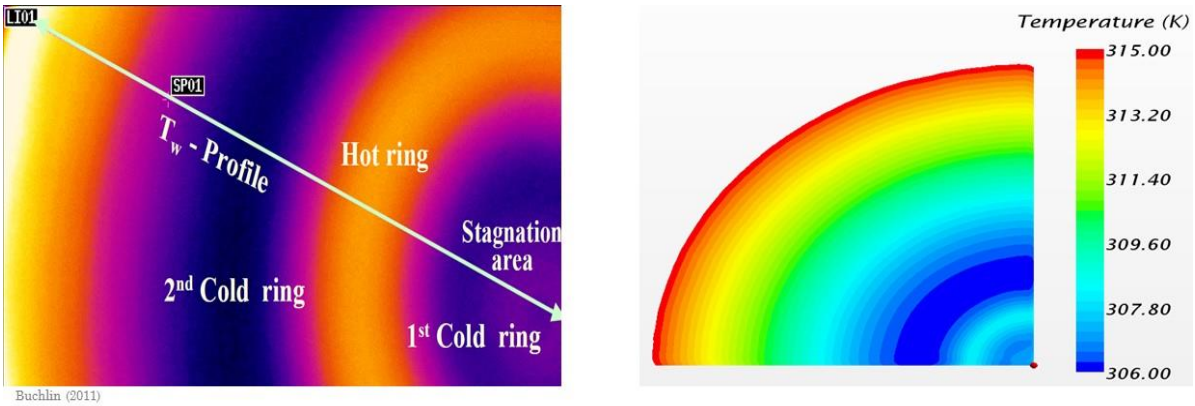

Figure 4.7: CFD Temperature Countour Comparisons

Noticing the location and magnitudes of the heat transfer rate peaks, they are attributed to the entrained air caused by added vortex rings in the shear layer of the turbulent impinging flow. This has been similarly seen by O'Donovan & Murray (2007). Figure 4.8 displays the flow ejected from the jet orifice. A radial acceleration zone just after the stagnation point and a wall flow build up which creates a secondary flow detachment region as r/D increases ultimately causing a heat transfer decrease are observed. The flow is then reattaching along the wall jet and increased heat transfer is identified in Figure 4.9. This is known to be a complex feature of impingement cooling.

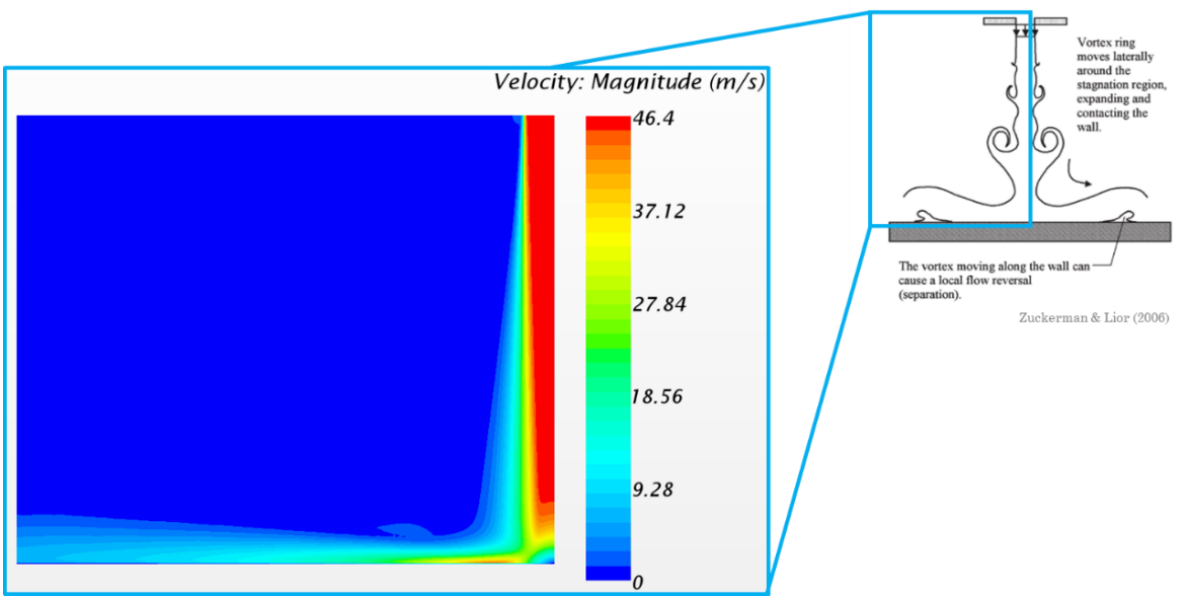

Figure 4.8: Flow Phenomenon

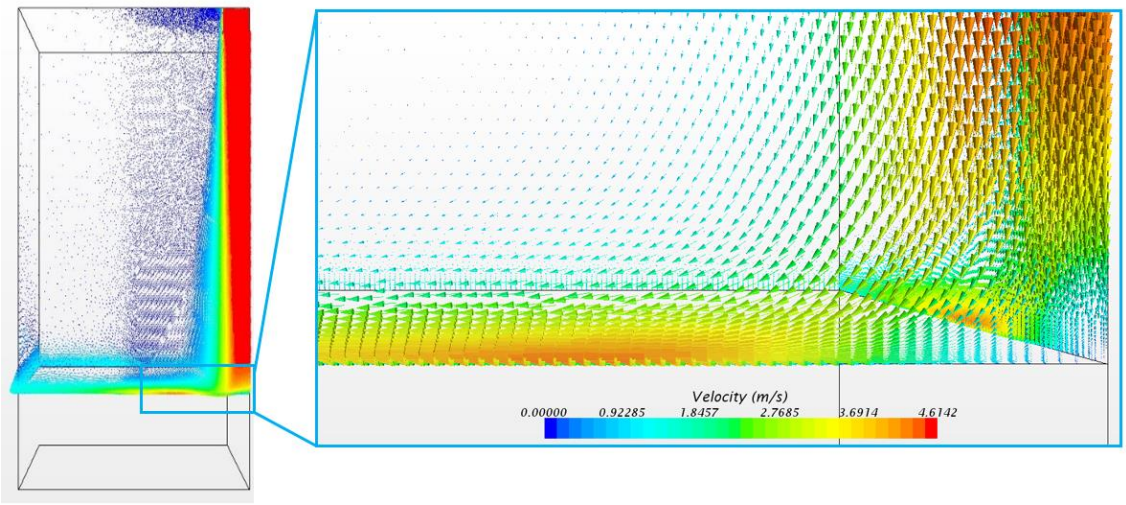

Figure 4.9: Velocity Streamlines of Flow

As stated by Curkurel (2015), when a high Reynolds number flow is introduced, the shear layer vortex formation and local heat transfer implications will be highly influenced by this high velocity fluid flow. A resulting delayed wall separation occurs due to the complexity of the mixing. Increased turbulence is caused by an unsteadiness in the thermal boundary layer outside of the stagnation region which decreases the heat transfer. Upon transition to the fully turbulent wall jet, the heat transfer distribution increases to a

secondary peak. Abrupt increases in the wall jet turbulence explains the location and magnitude of the secondary peaks observed (O'Donovan & Murray, 2007). This turbulence transition is displayed through the velocity profile of the flow field along with the turbulent kinetic energy (TKE) with respect to the radial distance within the control volume. An increasing shear force in the thin acceleration region immediately outside the stagnation zone is seen as a result the transition. Note that the location of the highest TKE adjacent to the wall correlates to the location of a secondary temperature increase (Zuckerman & Lior, 2006). This is observed in Figure 4.10, which depicts Nu and TKE along the side symmetry planes and the bottom heated surface respectively.

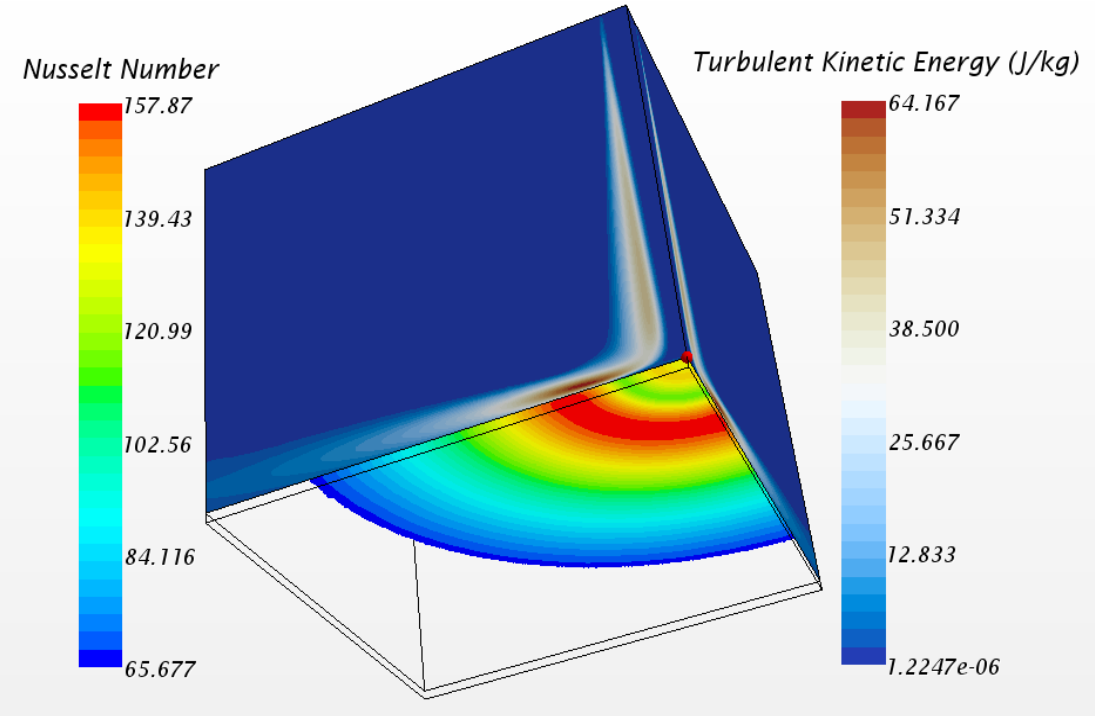

Figure 4.10: Turbulence Transition

4.2.6. Conclusions

An initial study for the fluid domain of a SRN jet impingement configuration has been analyzed. The mathematical and computational models created are compared to the work described predominantly by Martin (1977), Zuckerman and Lior (2006, 2007), and Buchlin (2011). Resulting heat transfer rates, primarily the Nusselt number, display varying values from those predicted in Martin's work.

Although there is a 33% under prediction rate at the stagnation point, overall heat transfer rates involving jet velocity, diameter and temperatures show promising results throughout the stagnation wall jet region along the target heated wall. These ranges are within trusted literary percentages. However, the turbulence effects of a high Reynolds number jet located at a high experimental height has proposed complications. With a Reynolds number of 48,361, the fluid flow causes detachment and reattachment zones outside of the stagnation region; a region which is known to give reduced heat transfer. It is noticed that at these zones concentric temperature regions are occurring due to the nature of the turbulent flow.

4.3. CHT Study

Next, further CFD analysis for this SRN air impingement model was conducted with an added thin-walled, solid material to the bottom of the fluid domain. This is to simulate more realistic heat transfer predictions for future comparisons for the rocket application portion of this study. A quarter model domain is again used for minimal computational cost and time.

4.3.1. Additions to the Computational Model

Having studied the impingement fluid domain for a Z/D of 7.5 at Re = 48,361, an acrylic, thin-walled solid is added to the bottom surface of the fluid domain. Acrylic was chosen for its low thermal conductivity (k) of 0.2 W/m2*K and ability to be readily available for in-house testing. A smooth wall assumption is used for simplicity. The wall thickness (th) was chosen as 3.175 mm to simulate attainable experimental dimensions for future in-house experimental testing.

With the addition of the solid domain, a contact interface was needed between the fluid flow and solid wall regions. A contact interface allowed the energy conservation and momentum between the domains to be transferred. Upon remeshing the combined domains, an additional 2 million cells were added as a result of the solid material. This resulted in a final CHT cell count of 7.3 million, shown in Figure 4.11.

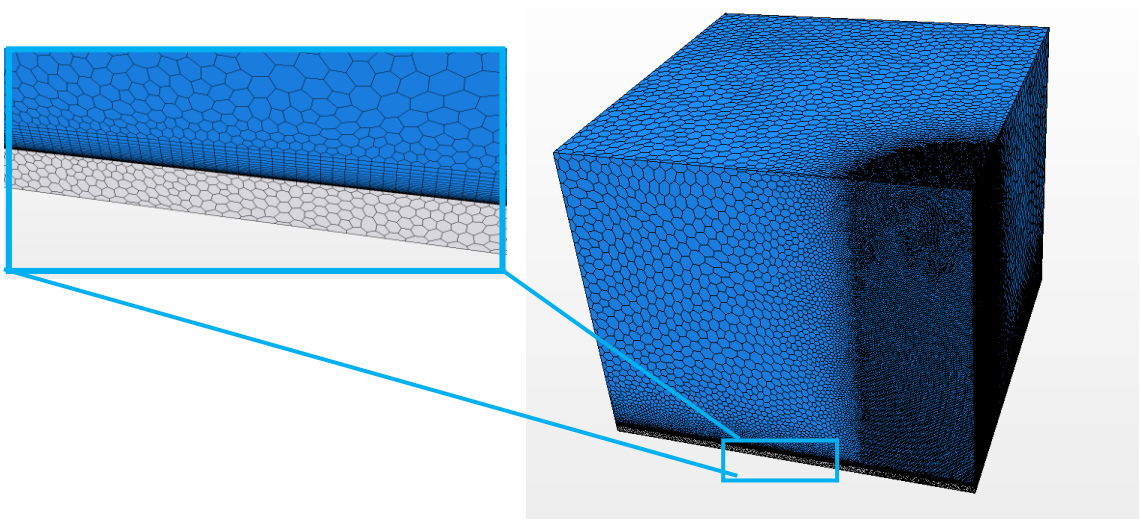

Figure 4.11: Fluid and Solid Domain Mesh Model, with Boundary Layer Cells

The same fluid domain parameters for a 300 K cool air jet as described above in sub-section 4.2.1 were again implemented for this model. However, with the added solid domain additional model continuum were required. For simplicity, the convective hot gas

side heat transfer rates were set as constant values along the bottom of the solid material. For the case of air impinging onto an acrylic flat plate, a bottom surface hot gas temperature (T_g) of 350 K was chosen for placement into Figure 3.1. This value was chosen to match temperatures commonly seen within experimental research. When inserted into Equation 13, with the same heat flux value of 1600 W/m^2 as the fluid domain, a resultant hot side heat transfer coefficient (h_g) of 31.9 W/m^2*K was obtained. This final value was placed into the CHT CFD simulation as a constant input on the bottom of the solid surface.

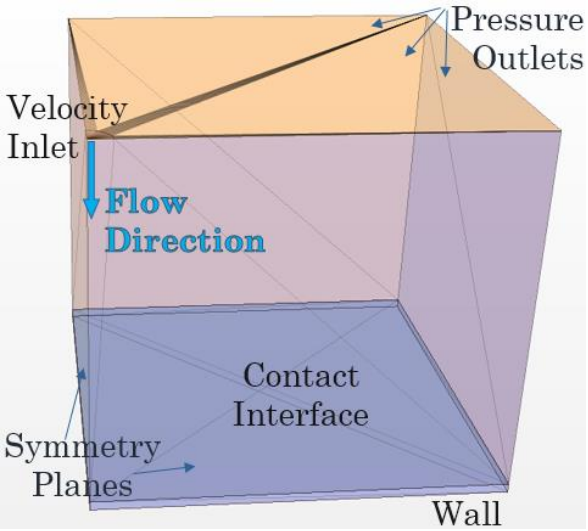

Figure 4.12: Fluid and Solid Computational Domain Setup

4.3.2. Results

Analyzing the updated simulation with the RANS v^{2}f turbulence model, chosen from analysis completed in sub-section 4.2.3, the resulting Nusselt numbers over a range of r/D from 0 to 7 were extracted from the CHT simulation. To compare these results to the non-CHT values, a plot of both trends with the literary values (Martin, 1977) included is given in Figure 4.13. Additionally, a constant temperature simulation was evaluated for comparison purposes.

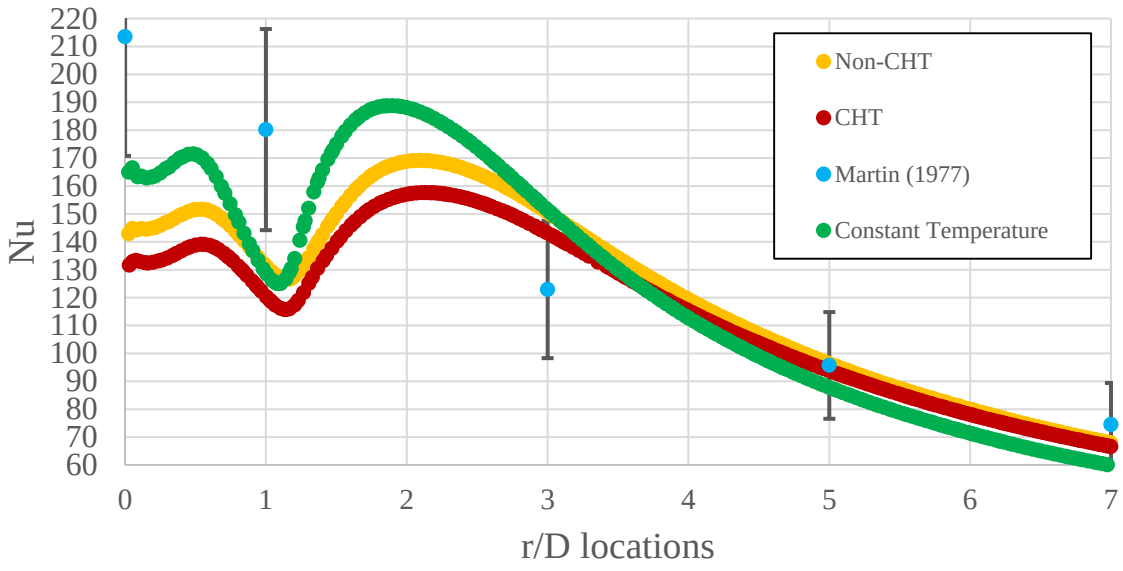

Figure 4.13: Heat Transfer Plot: r/D vs. Nu Comparisons for Benchmark Study

The difference in simulations is the addition of a solid material and a mixed boundary condition. Although both studies follow the same fluid domain parameters, it was found that for the simulations relative to each other, the CHT study showed an 8% decrease at the stagnation point, with improved comparisons moving radially outwards towards the other r/D locations of 1, 3, 5, and 7. This is contributed to the differences in the wall thermal boundary layer development due to the varying boundary conditions. The same general trend is observed between the two simulations, establishing confidence in the CHT simulation study conducted. There is still poor matching within the stagnation region, and a secondary peak again occurring at r/D = 2.2. Moving radially outwards from here, the Nu values show improved rates compared to Martin (1977).When assessing the air and acrylic CHT Nu results to that of Martin (1977), there is still a vast under prediction at the stagnation point. Table 4.2 shows the values and percent differences between the CHT CFD simulation and Martin's results (1977).

Table 4.2: Nusselt Number Values at Re = 48,361 for CHT case

r/D location	Nu, Non-CHT CFD	Nu, Martin (1977)	Nu, CHT CFD	% Difference between Martin & CHT
0 Stagnation Pont	142.9	213.5	131.6	38%
1	130.9	180.2	120.3	33%
3	150.1	122.9	143.1	16.6%
5	96.4	95.7	93.9	1.9%
7	68.2	74.5	67.9	8.9%

4.3.3. Analysis

With the similarity between simulations, there is a noticeable correlation in the various contours extracted from the CFD simulation. The temperature contour at the contact interface due to the temperature conduction effects between the domains, presented in Figure 4.14, depicts similar temperature fluctuations as that of the solely fluid domain previously shown in Figure 4.7. This again resulted in concentric hot and cold rings which move radially outwards, away from the stagnation region. The location of these rings once more matched to the location of the vortex rings in the shear layer of the turbulent fluid flow over the solid. The addition of the solid domain effects the temperature values slightly, improving the stagnation temperature by decreasing it 0.88% from 307.4 K to 304.7 K.

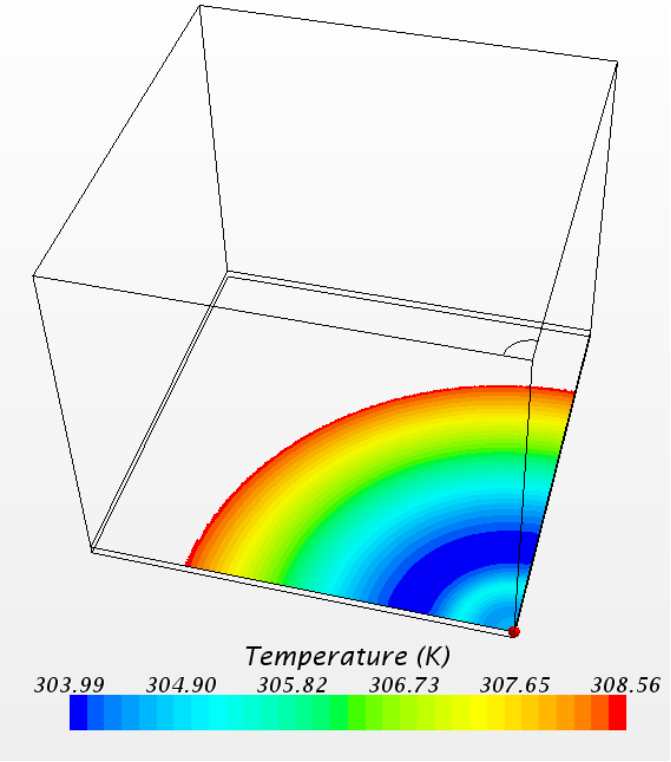

Figure 4.14: CHT Study Temperature Contour at Domain Interface up to r/D of 7

4.4. Final Remarks of Benchmark Model

Upon completion of a CFD CHT simulation modeled for fluid (air) and solid (acrylic) domains of a quarter SRN jet impingement configuration at a Z/D of 7.5 and Reynolds number of 48,361, the following conclusions are made:

- There is a 38% under prediction rate occurring at the stagnation point, which is a 7.9% increase from the non-CHT study stagnation Nusselt number. Due to the developing thermal boundary layer at the wall, this value is still within acceptable literary range (Zuckerman & Lior, 2006).
- With the aid of the v^2f CFD turbulence model, there is a noticeable secondary Nusselt number peak occurring at r/D = 2.2.
- For a Z/D of 7.5 at Re = 48,361, the fluid flow from the impinging jet can

create additional turbulence effects as it flows perpendicularly downwards onto the solid surface and moves radially away from the stagnation region. As a result, flow detachment and reattachment zones occur along the solid surface which generate concentric hot and cold temperature regions. These alternating regions result in lower predictions of the heat transfer rates in the stagnation zone.

- The addition of the acrylic solid domain reduced the cool surface temperature slightly, decreasing the value 0.88% from 307.4 K to 304.7 K.

5. Rocket Nozzle Model

5.1. Introduction

Having gathered data and gained confidence in the completed benchmarked CHT study, which models a gas turbine air SRN impingement configuration, a comparable rocket nozzle study is conducted. To the author's best knowledge, there has not been prior research conducted for a regeneratively cooled rocket nozzle utilizing jet impingement cooling. This assumption is based upon the extensive literature review conducted. The remainder of this study will focus on applying the benchmarked CHT model to an impinging cooling geometry with parameters similar to the SSME, with a focus on the nozzle throat region.

5.2. Rocket Model Setup

Many of today's highly pressurized LPREs are designed with a regenerative cooling system. The system is commonly coupled with a secondary cooling method, primarily film cooling, as regenerative cooling alone is not always sufficient (Yang, 2004). This study aims to investigate the feasibility of impingement cooling within a regenerative system. Combustion parameters for a full-scale SSME of 1860 kN thrust engine having cryogenic liquid oxygen (LOX) oxidizer and supercritical liquid hydrogen (LH2) fuel, with the LH2 used as the system's coolant, were implemented.

5.2.1. Hot Gas Side Calculations

To simplify the problem and concentrate on the heat transfer phenomenon occurring for the cooling portion of the rocket engine, the combustion was not modeled. Instead, the hot combustion gas produced along the bottom of the solid domain, outlined

in Figure 5.1, has been prescribed as a convective boundary condition to the rocket nozzle wall. The thermal properties of the combusted gases are extracted from the NASA Chemical Equilibrium with Applications (CEA) code (NASA Glenn). The required variables for hot gas side calculations are tabulated below in Table 5.1. For this study, the convective heat transfer coefficient (h_g) and assumed gas temperature (T_g) are set as input boundary conditions on the hot side of the CFD simulations on the bottom of the nozzle wall.

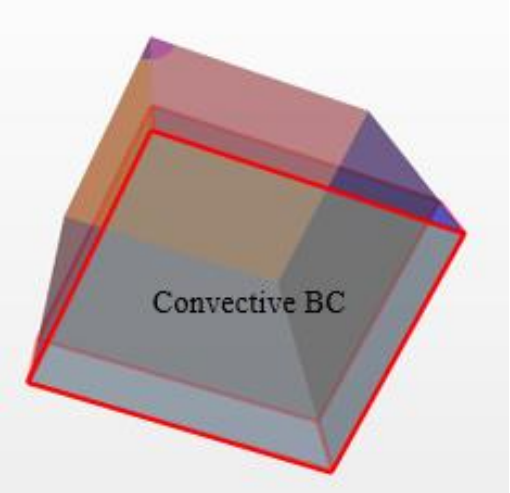

Figure 5.1: Hot Gas Side of Rocket Model

Table 5.1: Selected Combustion Properties from NASA CEA

	Units	Chamber	Throat
Pressure (P)	Pa	2.07E7	1.18E7
Temperature (T)	K	3604.2	3387.9
Specific Heat (c_p)	J/kg*K	6739.3	7354.9
Prandtl Number (Pr)	-	0.5587	0.5621
Dynamic Viscosity (μ)	Pa*s	1.04E-4	1.09E-4

The convective heat transfer rates within the combustion chamber to the nozzle wall must be calculated to properly model the hot gas side. Concentrating on the nozzle

throat region, the adiabatic wall temperature (T_{aw}) is calculated using Equations 17 and 18 with a specific heat ratio (γ) of 1.14 and Mach number (M) of 1. The resulting adiabatic wall temperature is thus 3561 K. The hot gas side heat transfer coefficient (h_g) is calculated using Equations 19 and 20. The SSME throat diameter (D*) is known to be 0.27 m with a characteristic velocity (C*) of 2320.8 m/s. As values are taken with respect to the nozzle throat region, it is noted that the value of $(D^*/r_c)^{0.1}$ is close to unity, and the area ratio $(A^*/A)^{0.9}$ is very close to 1. For this study, the effects of the nozzle curvature on the heat transfer coefficient are ignored. A resulting empirical convective h_g value was thus calculated to be 508,716 W/m2*K.

5.2.2. Coolant Properties

The heat transfer between the coolant and nozzle wall is generated by forced convection of the impinging jet. Influenced by the coolant chosen, the pressure and wall temperature can vary greatly depending on the phase of the fluid. For this study, liquid hydrogen (LH2) is studied in its supercritical phase. Liquid hydrogen has a known critical point located at T= 32.97 K and P=1.3 MPa. However, the pressure and temperature inside the cooling channels of a rocket engine are above those two values (DiValentin & Naraghi, 2010). Liquid hydrogen is at pressures higher than critical throughout the passage so that no boiling will take place (Hill & Peterson, 1992). Its temperature is below critical at the inlet and above critical at the outlet of the coolant passage. Thus, the liquid hydrogen in the coolant passage always has to pass through its pseudocritical temperature. Although a phase change does not occur at supercritical pressures, large changes in the transport properties do occur with very small changes in temperature near the pseudocritical temperature (Schacht & Quentmeyer, 1973). As a result, liquid hydrogen in a SSME setup

functions within its supercritical regime, with careful consideration taken to the temperature and the chosen pressure values.

Investigating hydrogen's supercritical properties, combined with a review of the literature, the coolant inlet temperature and pressure were chosen as input boundary conditions in the fluid domain. The coolant was ran as a constant density so that it could assume the LH2 coolant to be homogeneous for simplistic calculations. The fluid pressure is measured as 1.2 times the chamber pressure (P_{ch}), which resulted in 24.8 MPa. The inlet temperature is taken as 52.4 K, which was chosen to be comparative to values selected by research conducted by Wang *et al.* (1994). They studied the hot and cold side heat transfer of an LPRE combustion chamber of the SSME, similar to those studied in this paper.

5.2.3. Material Properties

While the fluid domain is driven by convection, the wall materials are predominately affected by conductive heat transfer. Four potential nozzle wall materials, Stainless Steel (SS 304), Inconel (Inconel x-750), copper and Acrylonitrile Butadiene Styrene (ABS) plastic, were investigated. Industry studies have begun to investigate the ability of utilizing 3-D printed thermoplastic resins, therefore ABS plastic was investigated to simulate a thermoplastic resin and analyze its effects within a rocket impingement cooling configuration. These materials were chosen for their range of thermal conductivities (k). Generally, a higher thermal conductivity value is preferred due to the reduced material thermal resistance. Utilizing the TSPX (NASA) and MatWeb material resource pages, the material properties were found and are displayed in Table 5.2.

Table 5.2: Investigated Wall Material Properties

	Units	SS 304	Inconel x-750	Copper	ABS Plastic
Density (ρ)	kg/m^3	7900	8280	8940	1060
Specific Heat (c_p)	J/kg*K	477	439	386	1424
Thermal Conductivity (k)	W/m*K	20	12	398	0.19
Linear Thermal Expansion Coefficient (α)	1/K	1.73 E-5	1.26 E-5	1.65 E-5	7.38E -5
Tensile Strength (σ)	MPa	505	310	210	40
Modulus of Elasticity (E)	GPa	193	213	117	2.2

A thin-walled nozzle wall material is desired so that the thermal stresses and high wall temperature faced will be minimal. By practice, a thin-walled rocket material is one whose thickness is less than or equal to 5% of the average chamber radius (Yang, 2004). Assessing for a SSME nozzle throat diameter (D*) of 0.27 m, the maximum wall thickness is 6.75 mm. The thickness of the solid remains at 3.175 mm, which is about 2.5% of the nozzle throat diameter.

5.3. Thermal Resistance Model Analysis

Evaluating the model for 1-D flow approximations provided an analytical model verification. For engine cooling, a reduction in material and coolant thermal resistance while minimizing the thermal gradients and stresses are desired. Referencing Section 3.3, the thermal resistance is analogous to electrical resistance models such that the resistance values across domains can be calculated.

To equate the resistance values for each domain, Equations 23 and 15 are utilized for the conductive and convective resistances, respectively. Using Equation 23 and a constant material thickness (th_{solid}) of 3.175 mm, the conductive resistances are displayed

in Table 5.3.

Table 5.3: Conductive Resistances of Selected Materials

	SS 304	Inconel x-750	Copper	ABS Plastic
R_{cond} (m^2*K/W)	1.59 E-4	2.65 E-4	7.98 E -6	1.67 E-2

The convective resistances are dependent on the heat transfer rates. Typically within a regenerative system, smooth channel flow is utilized. This study will additionally investigate an impingement setup on the coolant side, comparing values at the stagnation point.

5.3.1. Smooth Channel vs. Impingement Cooling Resistances

For the hot gas side, with a previously calculated heat transfer coefficient (h_g) of 508,716 W/m^2*K, the hot side convective resistance (R_{conv_hot}) was calculated as 1.97 E-6 m^2*K/W using Equation 15. For the coolant side, a preliminary step is required as the heat transfer coefficient is not yet known. To find this value, definitions for Nusselt numbers must be implemented dependent on the cooling flow method: smooth channel or impingement cooling.

For smooth channel flow, Equations 14 and 16 are set equal to each other with a Dittus-Boelter coefficient value of 0.023 and n exponent as 0.3 for a cooling fluid (Bergman & DeWitt 2011). A coolant heat transfer coefficient was (h_{cool}) calculated to be 11,467 W/m2*K. With this value, the coolant convective resistance (R_{conv_cool}) was thus calculated to be 8.72 E-5 m2*K/W.

For impingement, the log scale data plot from Martin (1977) seen in Figure 2.2 is utilized. The slope of the line at r/D= 0 is found to be 0.0042, and using the relationship $Nu = Re * m * Pr^{0.42}$, the Nusselt number is calculated to be 190.9 for a

Reynolds number of 48,361. Taking this value and plugging it into Equation 14, an impinging heat transfer coefficient (h_{cool}) of 17,713.23 W/m2*K is calculated. This resulted in a 35.5% increase in the heat transfer coefficient. By Equation 15, a cooling convective resistance (R_{conv_cool}) of 5.65 E-5 m^2*K/W was calculated.

To find the total resistance (R_{tot}) of each material model, the sum of the two convective resistances and respective conduction are added. All resistance values for both cooling configurations are displayed in Table 5.4. It can be seen that the impinging flow gave slightly lower total resistance values per material, except for the ABS plastic where the value remains the same. This is contributed to the low thermal conductivity (k) of 0.19 W/m*K associated with this thermoplastic resin.

$$\sum R = R_{conv\_hot} + R_{conv\_cool} + R_{cond} \tag{25}$$

Table 5.4: Smooth Channel vs. Impingement Thermal Resistance Comparisons (m^2*K/W) at Re= 48,361

Smooth Channel	R_{conv_hot}	R_{conv_cool}	R_{cond}	R_{tot}
SS 304	1.97 E-6	8.72 E-5	1.59 E-4 E-4	2.48 E-4
Inconel x-750	1.97 E-6	8.72 E-5	2.65 E-4	3.54 E -4
Copper	1.97 E-6	8.72 E-5	7.98 E -6	9.71 E-5
ABS plastic	1.97 E-6	8.72 E-5	1.67 E-2	1.67 E-2

Impingement	R_{conv_hot}	R_{conv_cool}	$R_{conduction}$	R_{tot}
SS 304	1.97 E-6	5.65 E-5	1.59 E-4	2.17 E-4
Inconel x-750	1.97 E-6	5.65 E-5	2.65 E-4	3.23 E-4
Copper	1.97 E-6	5.65 E-5	7.98 E -6	6.6 E-5
ABS plastic	1.97 E-6	5.65 E-5	1.67 E-2	1.67 E-2

To solve for the total heat flux (q''_{tot}) for each material's hot surface, the temperature difference (ΔT) across the entire system is divided by the corresponding R_{tot} value found in Table 5.4. Subtracting the LH2 temperature, 52.4 K, from the combustion gas temperature, a total temperature difference of 3334.6 K was calculated. From Equations 12 and 15, the total heat flux (q''_{tot}) with respect to each material resistance is calculated by Equation 26.

$$q''_{tot} = \frac{\Delta T}{R_{tot}} \tag{26}$$

With these values, the wall surface temperature (T_{wall}) along the hot side portion of the thermal resistance was calculated. As the convective heat transfer is driving the surface temperature of the system, this is the main area of interest for heat transfer calculations within this study. From Equation 27 below, using the found hot gas resistance (R_{conv_hot}) of 1.97 E-6 m^2*K/W and a hot gas temperature of 3387 K, the surface temperatures per material for both cooling methods were calculated. Their values are displayed within Table 5.5 alongside each materials' melting temperatures (T_{melt}). A visual representation is given in Figure 5.2, showing impingement cooling will give slightly better results over smooth channel cooling.

$$T_{wall} = T_g - (q''_{tot} * R_{conv\_cool}) \tag{27}$$

Table 5.5: Smooth Channel vs Impingement Heat Flux and Temperature Comparisions at Re= 48,362

Smooth Channel	q''_{tot} (kW/m^2)	T_{wall} (K)	T_{melt} (K)
SS 304	13,450.25	3,360.6	1,723
Inconel x-750	9,426.45	3,368.5	1,703
Copper	34,326.59	3,319.5	1,360
ABS plastic	198.86	3,386.6	378

Impingement	q''_{tot} (kW/m^2)	T_{wall} (K)	T_{melt} (K)
SS 304	15,354.74	3,356.8	1,723
Inconel x-750	10,323.71	3,366.7	1,703
Copper	50,221.33	3,288.3	1,360
ABS plastic	198.86	3,386.6	378

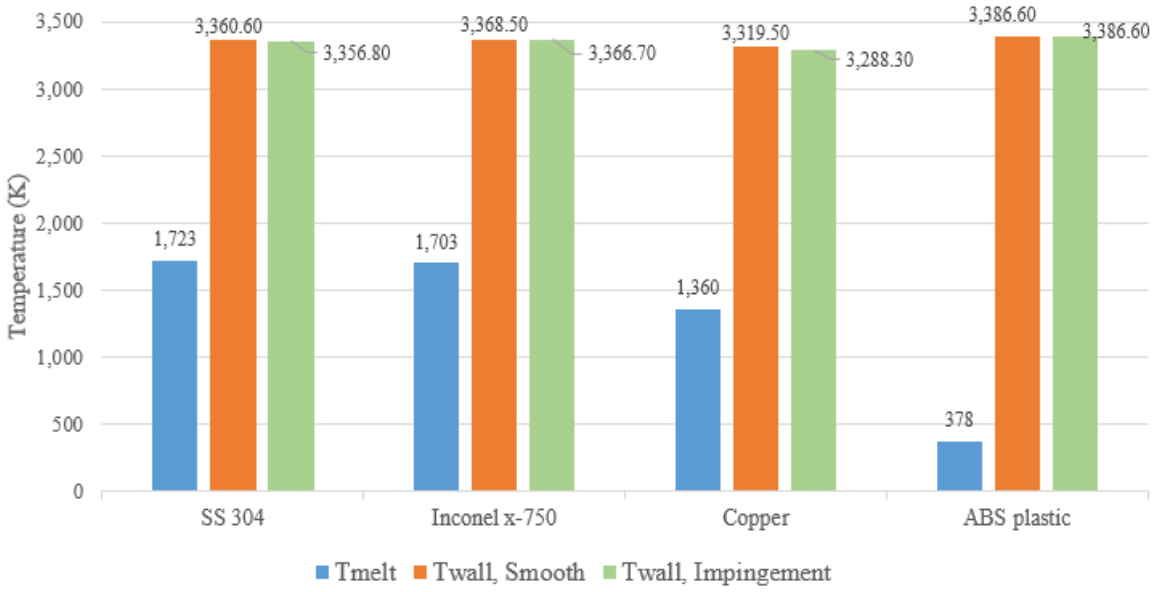

Figure 5.2: Smooth Channel vs. Impingement Comparision

Examining the results, it was noticeable that for either cooling method, all four materials will have their wall temperatures exceeding their respective melting temperatures by a wide margin. Compared to the smooth channel case, the impingement

analysis produced an increased coolant heat transfer coefficient, which resulted in a decreased convective resistance and thus lower total resistance. This in turn increased the total heat flux through the solid, which allowed the wall temperature to be slightly lower. However, it was not enough to overcome the extremely hot temperatures of the LOX/LH2 propellants. Even as the coolant resistances are pushed to infinity, all cases will fail. Therefore, further 1-D analysis was required.

5.4. Computational Model

For real-world application purposes, the CHT SRN model developed in the benchmark study (Section 4.3) at a Reynolds number of 48,361 is geometrically altered for more realistic jet-to-jet spacings. This is for future ARN configuration applications. A quarter jet domain is again utilized for decreased computational time. All fluid domain geometrical parameters were scaled down, however, it was important for a Z/D relationship of 7.5 to be maintained so that there can be accurate data comparisons between the rocket model and gas turbine CFD simulations. The jet-to-target spacing height (Z/D) were scaled down by 10%, and the streamwise (X) and spanwise (Y) distances were each scaled down 10% and then divided in half. This resulted in radial distances in both directions up to r/D of 4.5. This was done to better model the location between impinging jets where jet flow interactions will occur when applied to an array impingement configuration. At that location, added flow complexities in the impingement setup will arise. Therefore, in this study, the model simulates up to this location in the radial direction. A thin-walled solid is selected for all models remained at 3.175 mm. Table 5.6 summarizes the geometrical dimensions for each of the CHT models, with corresponding images displayed in Figure 5.3.

Table 5.6: Geometrical Comparisions between CHT Simulations

	D (mm)	Z/D	X/D	Y/D	th (mm)
a) Benchmark Study	16.76	7.5	9	9	3.175
b) Rocket Study	1.676	7.5	4.5	4.5	3.175

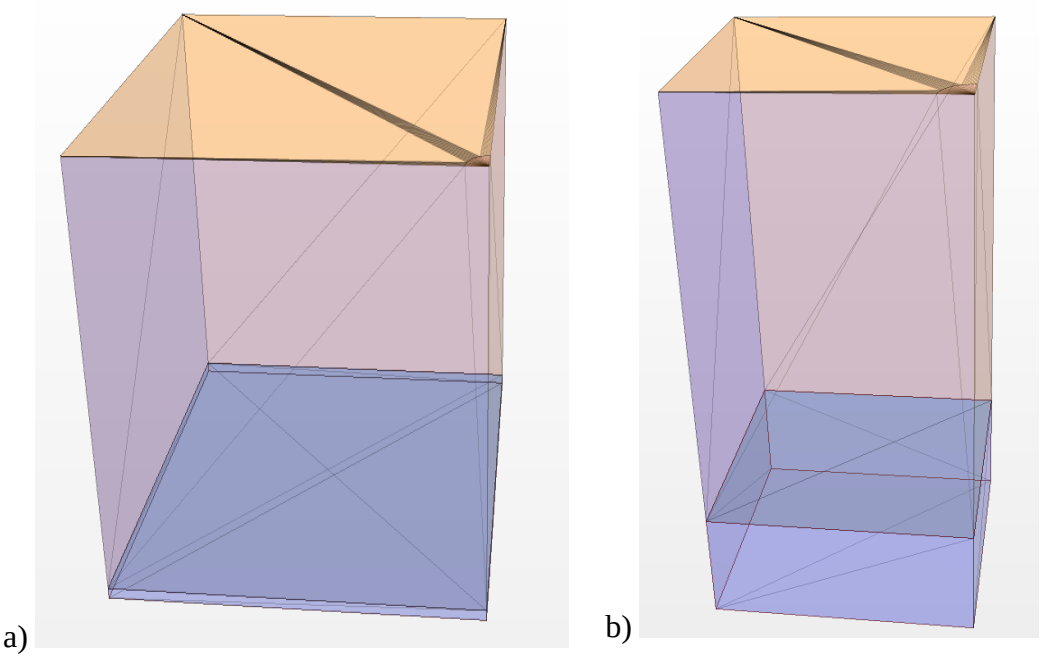

Figure 5.3: CHT Models Geometry Comparisons: a) Benchmark Study, b) Rocket Model

5.4.1. Meshing

The meshing models used for the rocket simulations remained the same as the CHT test conducted in Sub-Section 4.3.1. However, with the scaled down dimension decreases, a 10% decrease in the base and boundary layer thickness was implemented. As a result, base and boundary layer thickness values of 0.5 mm and 0.18 mm, respectively, were modeled. A comparison table of the mesh model inputs between the air and liquid hydrogen coolant simulations is given in

Table 5.7. A finer mesh of 0.03D, relative to the jet diameter, along the domain interface and fluid flow region is again used. A final rocket model mesh count of 4.9 million

cells was concluded as displayed in Figure 5.4.

Table 5.7: Mesh Model Input Comparision between Coolants

	Air	Supercritical LH2
Solver	Ideal gas	Liquid, constant density
Base Size (mm)	5	0.5
# Prism Layers	20	20
PL stretching	1.15	1.15
PL thickness (mm)	1.8	0.18
Surface Curvature (°)	60	60
Surface Growth Rate	1.1	1.1
Surface Size	25% base	25% base
Wall Thickness (mm)	$2.2x10^{-2}$	$2.2x10^{-2}$

Figure 5.4: Mesh Model of a Quarter Impinging Jet for a Rocket Nozzle Throat Cooling Geometry

5.4.2. Boundary Conditions

Keeping the jet Reynolds number at 48,361, the velocity inlet boundary condition is back calculated using fluid properties for supercritical liquid hydrogen at 24.8 MPa and 52.4 K. From the National Institute of Standards and Technology (NIST) Chemistry WebBook Database, the thermophysical properties of these parameters were found to be: density (ρ) of 69.35 kg/m^3 and dynamic viscosity (μ) of 1.1E-5 Pa*s. The coolant jet velocity was thus calculated to be 4.6 m/s. Using Equation 9, the mass flow rate ($\dot{m}$) through a single quarter jet of a 1.676 mm jet diameter is found to be 1.75 E-4 kg/s. Multiplying by four, a full single jet would have 7 E-4 kg/s. Assessing for an SSME model, the total mass flow rate of the impingement setup was calculated. Knowing the nozzle throat diameter (D*) is 0.27 m, spacing the jets 15.2 mm apart results in 18 array jets in a single row around the throat region. Not accounting for the radius of curvature but assessing for 15.2 mm jet spacing down along the 4.2 m length of the nozzle, 276 rows of jets would be manufactured. This would result to 4,908 total jets around a SSME nozzle, with a total mass flow rate of 3.4 kg/s. The SSME utilizes about 20% of its 467 kg/s LH2 for coolant in the regenerative cooling system (Miranda & Naraghi, 2011). With a 20% mass flow rate of 93.4 kg/s available for cooling, the impingement setup constructed in this study would be applicable for real applications.

The top and two outer sides are set to pressure outlet conditions, with the opposite inner two sides again as symmetry planes. These represent the sides where the remaining jet flow would be located. With the addition of a solid domain, a wall boundary is set along the bottom surface of the geometry and the contact interface is between the two domains. Figure 5.5 displays the rocket model CFD boundary conditions set forth in this study.

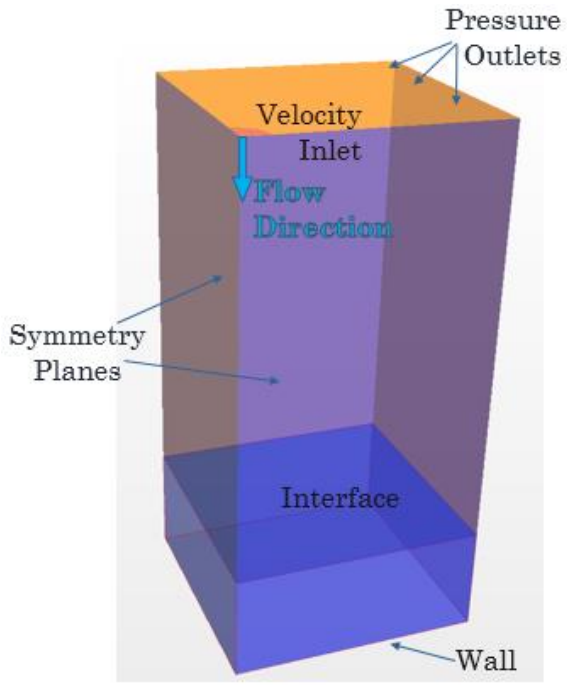

Figure 5.5: Rocket Model Boundary Conditions

5.5. Impingement CFD Results

Coupling the results of the 1-D thermal resistance analysis with 3-D computational analysis allowed for a better determination of an engine's optimal cooling design. Utilizing a 3-D, steady state, turbulent flow using RANS v^2f turbulence modeling with segregated flow and energy solvers within STAR-CCM+ CFD software, the heat transfer rates and temperature profiles for an SSME-like rocket nozzle cooling configuration is gathered. The data collected is compared to Nusselt number values extracted from Martin for $\frac{\overline{Nu}}{Pr^{0.42}}$, as displayed in Figure 2.2. However, the Nusselt number values must be updated to account for the rocket coolant in place of the previously found literary air values. Supercritical LH2, with a specific heat (c_p) of 12200 J/kg*K, dynamic viscosity (μ) of 1.1 E-5 Pa*s, and a thermal conductivity (k) of 0.15548 W/m*K, has Prandtl number (Pr) of 0.86 calculated from Equation 10. Evaluating the plot data for r/D = 0, 1, and 3, the literary values are

now 232.9, 196.5, and 134.1, respectively.

5.5.1. Nusselt Number Trends

CFD simulations were completed to demonstrate the fluid domain results between SS 304 and Inconel x-750 metals. The resulting Nusselt numbers over a range of r/D of 0 to 3 were extracted from the rocket CHT simulations. As seen below in Figure 5.6, the data is plotted with the Nusselt number trends for the SS 304 and Inconel metals with LH2 coolant. Similar to the benchmark CHT simulations, there is an under prediction at the stagnation point and an observable secondary peak at r/D of 2. This further confirms that the trends for a conjugate problem is indifferent to the fluid chosen for convective analysis.

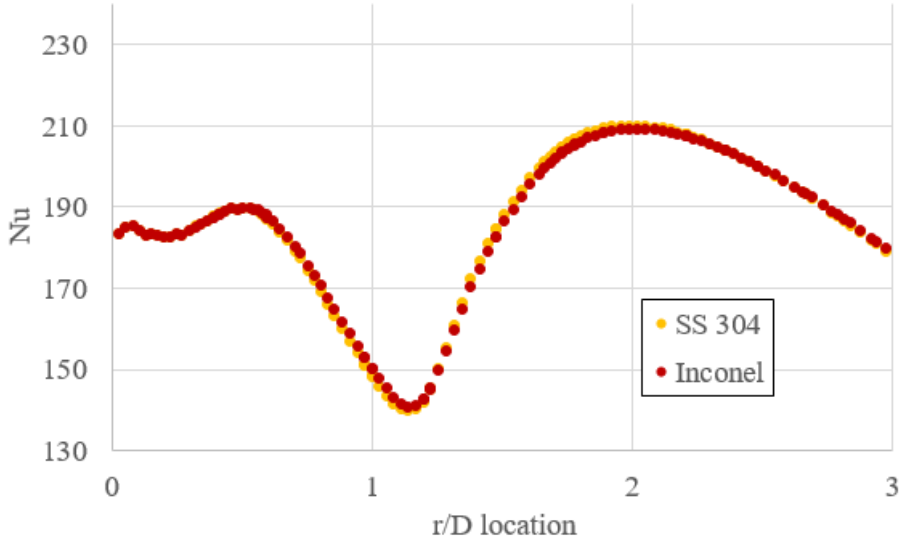

Figure 5.6: Heat Transfer Plot: r/D vs. Nu Comparisons for Rocket Simulations

It is found that for both metals considered here, they have an almost exact Nusselt number trend. This is expected due to the same fluid physics that is applied to all models. Nusselt number is a fluid parameter, based upon the fluid's heat transfer coefficient (h) and thermal conductivity (k) as shown in Equation 14. Each metal has a different thermal conductivity of either 12 or 20 W/m*K, which will produce different heat flux values and

thermal gradients. However, as the convective heat transfer coefficient is a proportionality constant between these two values, they will be the same. Additionally, the resulting Nusselt numbers will be equivalent. This is further shown by the values and percent differences in Table 5.8. Comparative to the benchmarked air CHT values in Table 4.2, the rocket simulations with LH2 coolant show a 45% increase of the stagnation Nusselt number.

Table 5.8: Nu Values for Supercritical LH2 at Re= 48,361 for Material Comparisons to Martin (1977)

r/D location	Martin (1977)	SS 304 CFD	% Diff.	Inconel x-750 CFD	% Diff.
0 Stagnation Pont	232.9	183.6	21.2	183.6	21.2
1	196.5	148.6	24.4	150.4	23.5
3	134.1	179.3	33.7	179.8	34.1

5.5.2. Impingement Models Analysis

As a supercritical fluid, the liquid hydrogen has a strong dependence on the temperature and pressure fields. Assuming a constant pressure of 24.8 MPa at the nozzle throat, the main driver for the heat transfer rates will be the temperature values. Incorporating solely impingement cooling to the CHT simulations, it is gathered that at the stagnation point, r/D = 0, the resulting temperatures of the metals will exceed their melting temperatures, as displayed in Table 5.9 and Figure 5.7.

Table 5.9: Metal Temperature Values from CFD Impingement Cooling with LH2 at T = 52.4 K at r/D = 0

	T_{melt} (K)	T_{wall} (K)	Temperature Difference (K)
SS 304	1,723	3,352.9	1,629.9
Inconel x-750	1,703	3,539.9	1,836.9

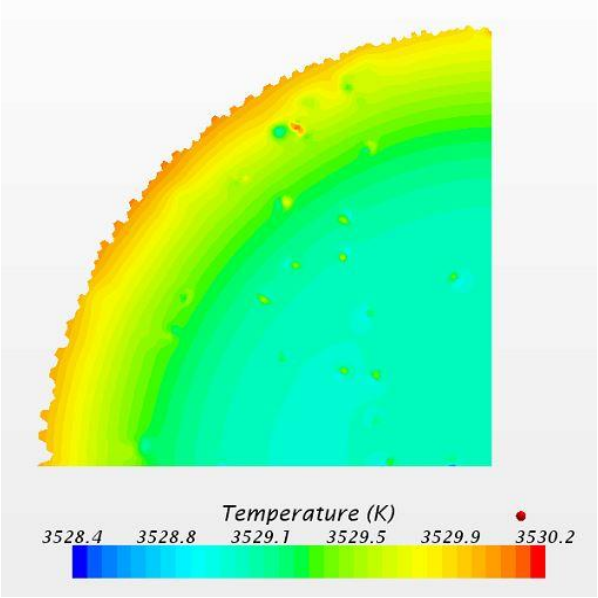

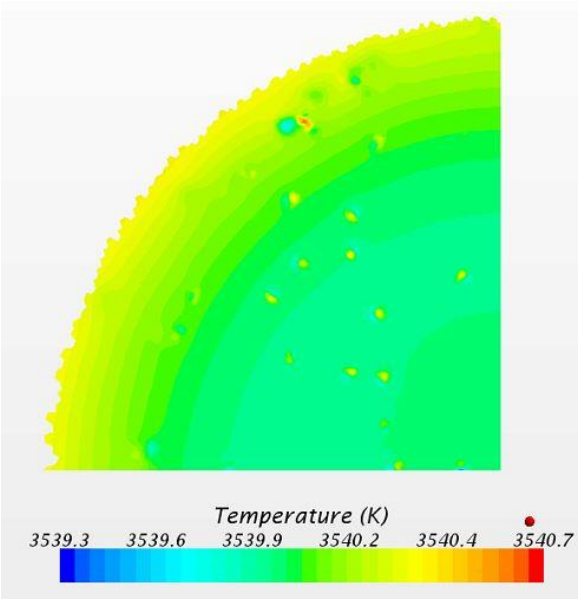

a) SS 304 b) Inconel x-750

Figure 5.7: Hot Gas SideTemperature Contours of LH2 Impinged Metals

With a hot gas side temperature of 3561 K applied to the bottom of the computational model, the resulting wall temperatures (T_{wall}) are over double the melting temperatures. This correlates to the 1-D analysis completed in Sub-Section 3.2.1. With the jet temperature at 52.4 K, each metal was barely cooled, which is unacceptable for real hot-firing rocket nozzles. Therefore, this concludes that the impingement cooling alone is not viable for a SSME-like rocket nozzle throat region and additional cooling method(s) are needed.

5.6. Concept Screening

To assess for a safe and usable material surface temperature, various variables of the 1-D thermal resistance analysis can be altered and re-examined. Comparing to the benchmark study conducted, an attempt to keep as many parameters constant is most ideal, with only one variant improved. Therefore, alterations to the wall thickness (th), jet

diameter (D_{jet}) and jet velocity (v_{jet}) are separately investigated.

To keep a Reynolds number of 48,361 for a 1.6 mm diameter jet, the materials' wall thickness was altered. To keep materials below their melting temperatures, it was decided that the wall thickness should be decreased from 3 mm to 0.1 mm. However, even with this decrease in thickness, none of the selected materials were able to stay below their melting temperatures. Although a thin-walled material is preferred, too thin of a wall thickness has the potential to lose the necessary strength to withstand the operating conditions of the engine. If there is an excessive stress on the walls, they are in danger of failing, especially at such high temperature gradients.

A study of the jet diameter variation was conducted by maintaining a Nusselt number of 191 for the supercritical LH2 coolant. Noted from Equation 16, as the jet diameter decreases, the heat transfer coefficient will increase. As a higher heat transfer coefficient is desired for resistance calculations, a decrease in the jet diameter was studied. By doing so, it was determined that even a diameter decrease from 1.6 mm to below 1 E-9 mm would still be not be sufficient to decrease the surface temperatures below their melting points. As this value is unrealistically small for viable testing applications, it was concluded that all materials would still fail with a decreased diameter.

By varying the jet velocity, the Reynolds number properties for the supercritical LH2 coolant was be conducted. Again, there is a need to keep the resulting temperature below the material melting temperatures. It was found that even if Reynolds number was to increase towards infinity, an applicable impingement setup cannot be achieved.

After an in-depth assessment of a 1-D analysis for a regeneratively cooled rocket nozzle throat region coupled with impingement cooling was completed, it was concluded

that for similar combustion chamber dimensions and gas properties to the SSME with a Re = 48,361 at an impinging height-to-diameter ratio of 7.5, impingement cooling alone is not feasible. Keeping for the chosen parameters modeled in by gas turbine cooling, the resulting values are not capable of cooling a rocket engine by itself. Although impingement cooling is commonly used within gas turbine cooling, the high temperature of a LPRE are insufficiently cooled. With combustion temperatures rising towards 3500 K and material temperature limits below 2000 K, the materials will fail under the predisposed conditions. To better cool the system, an additional cooling technique will need to be incorporated into the design in order to help keep the hot gas side wall temperatures low.

Investigating cooling techniques for both gas turbine and rocket engines, many methods will couple with either a thermal barrier coating (TBC) or film cooling. As researched by Miranda & Naraghi (2011), pure supercritical hydrogen will give an increase to the film cooling within a regenerative system. Therefore, film cooling was simulated to the impingement setup and analyzed for its feasible assistance to cool an engine.

5.7. Film Cooling

Film cooling is a known cooling method which reduces the heat transfer through walls which reduces the thermal stresses on the material by providing a thin, cool film over the solid (Huzel & Huang, 1992). Utilizing a film cooling technique to aid heat augmentation on the inner side of the nozzle throat, an analysis for added film cooling effectiveness (η_{eff}) is conducted. Ideally, a cooling effectiveness of 1 would symbolize that the driving parameter, the adiabatic wall temperature (T_{aw}), is equivalent to coolant temperature. A low η_{eff} represents an insufficient cooling application on behalf of the film

cooling method. For the chosen SSME parameters, the effectiveness is calculated to be 0.01 as defined by Equation 28. This signifies if film cooling was to be placed within the simulations as is, it will not help to increase the temperature difference of the materials.

$$\eta_{eff} = \frac{T_g - T_{aw}}{T_g - T_{cool}} \tag{28}$$

5.7.1. Impingement & Film Cooled Model Analysis

To be able to incorporate a film cooling technique to the impingement rocket CFD simulations, an assumed effectiveness value of $\eta = 0.5$ as seen in the literature was used for the hot gas side temperatures. Manipulating Equation 28 to solve for T_{aw} for CFD implementation, a corrected T_{aw} value of 1667.3 K was calculated. This was a 53% decrease from the original 3561 K temperature. The new adiabatic wall temperature allowed the same parameters, such as Re, D, and h_g, to be the conditions used in later simulations further discussed in this study. From the updated 1-D analysis, using Equations 26 and 27, the total heat flux (q''_{tot}) and surface temperatures for the three metals are given in Table 5.10, along with their respective melting temperatures. Although the material will soften and fail prior to reaching its melting temperature, this temperature was chosen as the failing temperature for preliminary analysis.

Table 5.10: Heat Flux and Temperature Comparisions for Impingement with Film Cooling

Impingement & Film Cooling	q''_{tot} (W/m^2)	$T_{w\ all}$(K)	T_{melt} (K)
SS 304	7,393,530	1,652.8	1,723
Inconel x-750	4,967,587.7	1,657.5	1,703
Copper	24,298,496.4	1,619.5	1,360

As seen in Table 5.10, it was revealed that only SS 304 and Inconel x-750 would be able to withstand the temperatures within the model. Therefore, only these two metals were analyzed more in depth throughout the remainder of this study. Evaluating the CFD simulation of SS 304 and Inconel x-750, their resulting temperature contours are displayed in Figure 5.8.

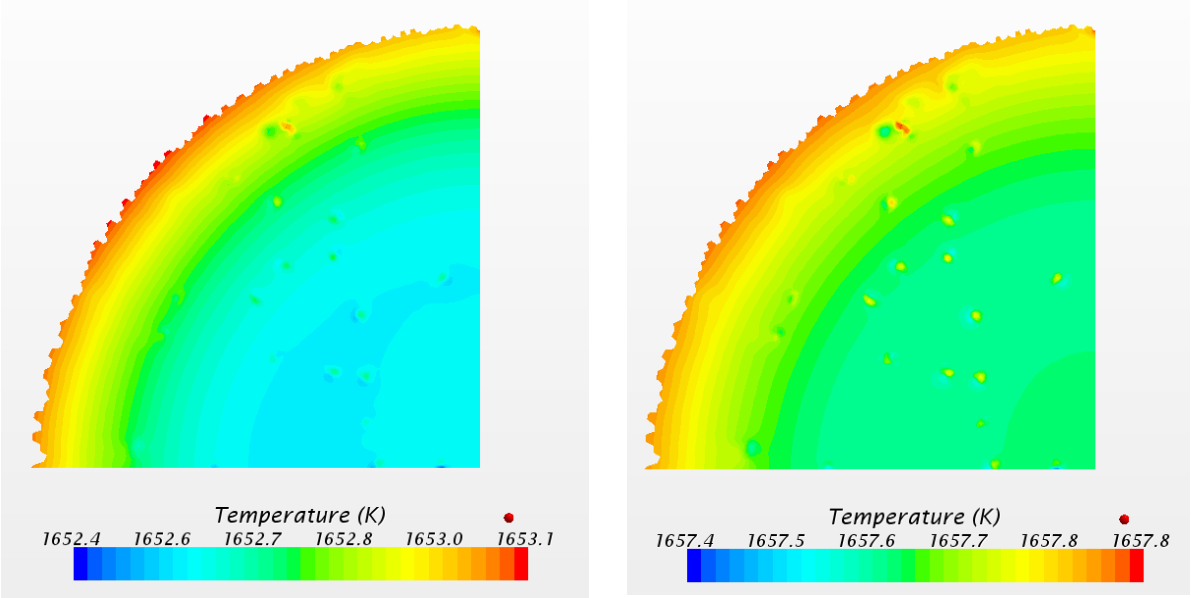

a) SS 304 b) Inconel x-750

Figure 5.8: Metal Hot Gas SideTemperature Contours with Added Film Cooling

Comparing the metals for their impingement cooled models from Sub-Section 5.5.2 with the combined cooling models discussed above, Figure 5.9 displays the wall temperatures by 1-D analysis and CFD simulations. Graphing in relation to the metals' melting temperatures, it is seen that with the addition of film cooling, both metals are capable of staying below this failing temperature. Additionally, analyzing between the 1-D and CFD models, again there is little difference between the temperature values. This further concludes that 1-D analysis is sufficient and an in-depth conjugate analysis is not necessary for future work.

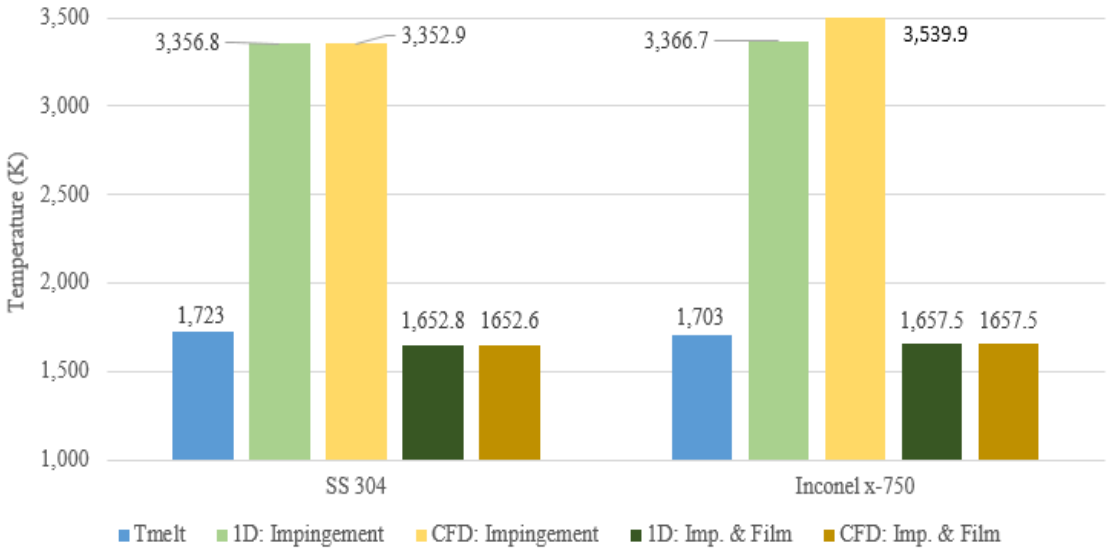

Figure 5.9: Impingement vs. Film Cooled Model Comparisions

6. Project Conclusion

A novel heat transfer study is completed, which investigated the feasibility of a jet impingement cooling technique for a regeneratively cooled rocket nozzle. The nozzle throat region resembling that of the Space Shuttle Main Engine (SSME) was investigated. An empirical model constructed from research based on Martin's model (1977) was developed for a single round jet (SRN) at a Reynolds number (Re) of 48,361 with a height-to-target-plate (Z/D) distance of 7.5. A benchmark model of 300 K air coolant was first assessed and its Nusselt number (Nu) and temperature profiles were analyzed.

It was found that for an air cooled CHT model, there is a 38% under prediction rate of the Nusselt number (Nu) at the impinged stagnation point when compared to Martin's paper (1977). As the radial distance (r/D) increased, values with ranges within trusted literary percentages improved. However, the turbulence effects of a high Reynolds number jet located at a high experimental height has caused complications. The fluid flow caused detachment and reattachment zones outside of the stagnation region, a region which is known to give reduced heat transfer rates. A decrease in Nu value occurred at r/D of 1.2 with a secondary peak around r/D of 2. It was noticed that within these fluctuating zones there were concentric temperature regions occurring due to the turbulent flow across the solid domain. These alternating regions resulted in overall lower heat transfer rates predicted within the stagnation zone.

Applying the information gathered from the benchmark study, the CFD model geometry was altered for more realistic rocket nozzle cooling dimensions by decreasing its fluid domain by 10%. Utilizing LOX/LH2 propellants for the hot gas side calculations, hot side heat transfer rates of a calculated convective heat transfer coefficient (h_g) of 508, 716

W/m2*K at a combustion temperature of 3387 K were applied. Supercritical LH2 coolant at 52.4 K and 24.8 MPa was investigated. To ensure the impingement setup would be applicable for a SSME, a mass flow rate analysis was evaluated and verified. A 1-D thermal resistance analysis was first conducted for four materials: Stainless Steel (SS 304), Inconel x-750, copper, and ABS plastic. Through this numerical analysis, and confirmed through CFD simulations, it was found that none of the selected materials are feasible with impingement cooling alone. This result was due to the high combustion temperatures inside the nozzle reaching upwards of 3561 K. The wall materials were only slightly cooled, with their resulting temperatures exceeding double their melting temperatures, which was considered the failing condition in this study. Therefore, all studied material were concluded to be capable of withstanding the high stresses that act on a hot-firing nozzle.

It was further concluded that an additional cooling method is required to help keep the hot gas temperatures low. Under SSME conditions, either a thermal barrier coating (TBC) or film cooling must be incorporated. To ease the thermal stresses on the remaining metals within this study, an assumed film cooling effectiveness value (η) of 0.5 was integrated into the hot gas side calculations to increase the hot side resistance. This decreased the hot side wall temperature to 1667.3 K, allowing the materials to be properly cooled on the inner side of the nozzle. Even with this added assisted cooling method, it was concluded through further additional 1-D analysis that only SS 304 and Inconel x-750 metals were capable of withstanding the rocket nozzle temperatures. The resulting values were slightly below their respective melting temperatures, concluding that film cooling cannot be eliminated from the system. CFD simulations for these two materials were studied and with confirmation of their cooled wall temperatures, it was conjectured that

lateral conduction effects will not have a major impact on the cooling system, therefore 1-D analysis will be sufficient for future analysis.

7. Recommendations

As the desire to keep material temperatures low for a more efficient engine, the need for improved cooling techniques is essential. Although impingement cooling alone is not feasible for a SSME-like rocket nozzle with LOX/LH2 propellants and SS 304 or Inconel x-750 metal wall materials, further analysis could allow impingement cooling to be feasible with different combinations. Alternative high thermal conductivity materials could be investigated, with LOX/LH2 or other propellants, and can be assessed for a similar SSME or different rocket nozzles. Additionally, a full analysis of an impingement with film cooling system could be studied to investigate the smallest percentage of film cooling that is needed. Besides film cooling, impingement with TBC could also be investigated. For both analyses, improved considerations of the turbulence effects of the impinging jet for the heat flux and temperature on the hot gas side wall would help to assess the totality of impingement cooling for a regeneratively cooled rocket nozzle throat.

REFERENCES

Al-Hadhrami, L. M., Shaahid, S., & Al-Mubarak, A. A. (2011). Jet Impingement Cooling in Gas Turbines for Improving Thermal Efficiency and Power Density. Advances in Gas Turbine Technology.

Bartz, D. R., (1957). A simple equation for rapid estimation of rocket nozzle convective heat transfer coefficients. Jet Propulsion, January, 49-51.

Bergman, T. L., & DeWitt, D. P. (2011). *Introduction to heat transfer* (6th ed.). Hoboken, NJ: Wiley.

Behnia, M., Parneix, S., & Durbin, P., (1997) Accurate Modeling of Impinging Jet Heat Transfer. Annual Research Briefs, Center for Turbulence and Research, NASA Ames/Stanford Univ.

Boyce, M. P. (2006). Gas turbine engineering handbook (3rd ed.). Houston, TX: Gulf Pub.

Brdlick,P.M. and Savin,V.K. (1965). Inzh.-Fiz.Zh. 8, 146.

Brown, T. *et al.* (1968). Evaluation of internal heat transfer coefficients for impingement cooled turbine airfoils. 4th Propulsion Joint Specialist Conference.

Buchlin, J. M. (2011). Convective Heat Transfer in Impinging-Gas-Jet Arrangements. *Applied Fluid Mechanics, 4*(1).

Bunker, R. S. (2007). Gas Turbine Heat Transfer: Ten Remaining Hot Gas Path Challenges. J. Turbomach. Journal of Turbomachinery, 129(2), 193.

CD-adapco, Computational Dynamics Analysis & Design Application, Star-CCM+, [Computer Software], Ver. 9.06.011, Orlando, FL. Retrived September, 2015.

Claretti, R. (2013). *Heat and fluid flow characterization of a single-hole-per-row impingement channel at multiple impingement heights* (Unpublished doctoral dissertation). U of Central Florida.

Coulbert, C. D. (1964). Selecting cooling techniques for liquid rockets for spacecraft. Journal of Spacecraft and Rockets, 1(2), 129-139.

Curkurel, B., Fénot, M., & Arts, T. (2015). Conjugate Jet Impingement Heat Transfer Investigation via Transient Thermography Method. Journal of Thermophysics and Heat Transfer, 29(4), 737-746.

Dees, J. E. (2010). *Experimental Measurements of Conjugate Heat Transfer on a Scaled-up Gas Turbine Airfoil with Realistic Cooling Configuration* (Unpublished doctoral dissertation). U of Texas.

Divalentin, J., & Naraghi, M. (2010). Effects Cooling Channel Curvature on Coolant Secondary Flow and Heat Transfer. *46th AIAA/ASME/SAE/ASEE Joint Propulsion Conference & Exhibit*.

Downs, J. P., & Landis, K. K. (2009). Turbine Cooling Systems Design: Past, Present and Future. Volume 3: Heat Transfer, Parts A and B.

Florschuetz, L. W., Truman, C. R., & Metzger, D. E. (1981). Streamwise Flow and Heat Transfer Distributions for Jet Array Impingement with Crossflow. Volume 3: Heat Transfer; Electric Power.

Gardon, R. and Cobonpue, J. (1962). Heat Transfer between a Flat Plate and Jets of Air Impinging on It. International Developments in Heat Transfer, pp. 454-460, ASME, New York.

Goddard, R. H. (1914). U.S. Patent No. US1102653. Washington, DC: U.S. Patent and Trademark Office.

Goldstein, R. J., Behbahni, A. I., Heppelmann, K. K. (1986). Streamwise distribution of the recovery factor and the local heat transfer coefficient to an impinging circular air jet, Int. J. Heat Mass Transfer Vol. 29, pp. 1227-1235.

Han, B. and Goldstein, R. J. (2001). Jet impingement heat transfer in gas turbine systems, in *Heat Transfer in Gas Turbine Systems*, Annals of the New York Academy of Sciences, Vol. 934, pp. 147-161.

Han, J., Dutta, S., & Ekkad, S. (2001). Gas turbine heat transfer & cooling technology. Washington, D.C.: Taylor & Francis.

Hill, P. G., & Peterson, C. R. (1992). Mechanics and thermodynamics of propulsion (2nd ed.). Reading, MA: Addison-Wesley Pub.

Humble, R. W., Henry, G. N., & Larson, W. J. (1995). Space propulsion analysis and design. New York: McGraw-Hill.

Huzel, D. K., & Huang, D. H. (1992). Design of liquid propellant rocket engines (Revised ed., Vol. 147). Reston, VA: American Institute of Aeronautics and Astronautics.

Hydrogen, H2, Physical properties, safety, MSDS, enthalpy, material compatibility, gas liquid equilibrium, density, viscosity, flammability, transport properties. (n.d.). Retrieved March 1, 2016, from http://encyclopedia.airliquide.com/Encyclopedia.asp?GasID=36

Hylton, L. D., Mihelc, M. S., Turner, E. R., Nealy, D. A., & York, R. E. (1983). Analytical and experimental evaluation of the heat transfer distribution over the surfaces of turbine vanes."*National Aeronautics and Space Administration, NASA Lewis Research Center*.

Kang, Y., & Sun, B. (2011). Numerical Simulation of Liquid Rocket Engine Thrust Chamber Regenerative Cooling. Journal of Thermophysics and Heat Transfer, 25(1), 155-164.

Kim, S., Joh, M., Choi, H. S., & Park, T. S. (2014). Effective Modeling of Conjugate Heat Transfer and Hydraulics for the Regenerative Cooling Design of Kerosene Rocket Engines. Numerical Heat Transfer, Part A: Applications, 66(8), 863-883.

Kuhl, D., J., Riccius, R., & Haidn, O. J. (2002). Thermomechanical Analysis and Optimization of Cryogenic Liquid Rocket Engines. Journal of Propulsion and Power, 18(4), 835-846.

Lee, J., Ren, Z., Haegele, J., Potts, G., Jin, J. S., Ligrani, P., . . . Moon, H. (2013). Effects of Jet-to-Target Plate Distance and Reynolds Number on Jet Array Impingement Heat Transfer. Volume 3A: Heat Transfer.

Ligrani, P. M., Oliveira, M. M., & Blaskovich, T. (2003). Comparison of Heat Transfer Augmentation Techniques. AIAA Journal, 41(3), 337-362.

Marchi, C. H., Laroca, F., Silva, A. F., & Hinckel, J. N. (2004). Numerical Solutions Of Flows In Rocket Engines With Regenerative Cooling. Numerical Heat Transfer, Part A: Applications, 45(7), 699-717.

Martin, H. (1977). Heat and Mass Transfer between Impinging Gas Jets and Solid Surfaces. Advances in Heat Transfer Advances in Heat Transfer Volume 13, 1-60.

Miranda, A., & Naraghi, M. (2011). Analysis of Film Cooling and Heat Transfer in Rocket Thrust Chamber and Nozzle. *49th AIAA Aerospace Sciences Meeting including the New Horizons Forum and Aerospace Exposition.*

Mensch, A., & Thole, K. A. (2014). Conjugate heat transfer analysis of the effects of impingement channel height for a turbine blade endwall. International Journal of Heat and Mass Transfer, 82, 66-77.

Moran, M. J., & Shapiro, H. N. (2011). *Fundamentals of engineering thermodynamics* (7th ed.). New York: Wiley.

Naraghi, M., Dunn, S., & Coats, D. (2006). Dual Regenerative Cooling Circuits for Liquid Rocket Engines. 42nd AIAA/ASME/SAE/ASEE Joint Propulsion Conference & Exhibit.

NASA Glenn (n.d.). CEARUN. Retrieved March 11, 2016. https://cearun.grc.nasa.gov/

NASA. (n.d.). Material Properties Database. Retrieved March 11, 2016, from https://tpsx.arc.nasa.gov/

O'Donovan, T. S., & Murray, D. B. (2007). Jet impingement heat transfer – Part I: Mean and root-mean-square heat transfer and velocity distributions. International Journal of Heat and Mass Transfer, 50(17-18), 3291-3301.

Oates, G. C. (1988). Aerothermodynamics of gas turbine and rocket propulsion. Washington, DC: American Institute of Aeronautics and Astronautics.

Online Materials Information Resource - MatWeb. (n.d.). Retrieved March 11, 2016, from http://www.matweb.com/

Petzold, K. (1964). Heat transfer on a perpendicularly impinged plate. Wiss. Z. Tech. Univ., Dresden 13, pp. 1157-1161.

Rahman, M. M., Bula, A. J., & Leland, J. E. (2000). Analysis of Transient Conjugate Heat Transfer to a Free Impinging Jet. Journal of Thermophysics and Heat Transfer, 14(3), 330-339.

Rajagopal, M. (2015). Numerical Modeling of Regenerative Cooling System for Large Expansion Ratio Rocket Engines. Journal of Thermal Science and Engineering Applications J. Thermal Sci. Eng. Appl., 7(1), 011012.

Rohatgi, A. (2015). WebPlotDigitizer (Version 3.9) [Web program]. Retrieved from http://arohatgi.info/WebPlotDigitizer/app/?

San, J., & Shiao, W. (2006). Effects of jet plate size and plate spacing on the stagnation Nusselt number for a confined circular air jet impinging on a flat surface. *International Journal of Heat and Mass Transfer, 49*(19-20), 3477-3486.

Schacht, R. L., & Quentmeyer, R. J. (1973). Coolant-side heat-transfer rates for a hydrogen-oxygen rocket and a new technique for data correlation. *Lewis Research Center*.

Schlünder, E. U. and Gnielinski, V. (1967), Wärme- und Stoffübertragung zwischen Gut und aufprallendem Düsenstrahl. Chemie Ingenieur Technik, 39: 578–584

Sforza, P. M. (2012). Theory of aerospace propulsion. St. Louis, MO: Butterworth-Heinemann.

Smirnov, V., Verevochkin, G., & Brdlick, P. (1961). Heat transfer between a jet and a held plate normal to flow. International Journal of Heat and Mass Transfer, 2(1-2), 1-7.

Sutton, G. P. (2003). History of Liquid Propellant Rocket Engines in the United States. Journal of Propulsion and Power, (19.6).

Sutton, G. P. (2000). *Rocket propulsion elements: An introduction to the engineering of rockets* (7th ed.). New York: Wiley.

Taylor, T. S. (2009). Introduction to rocket science and engineering. Boca Raton, FL: CRC Press.

Turner, M. J. (2010). Rocket and spacecraft propulsion principles, practice and new developments (3rd ed.). Berlin Heidelberg: Springer.

U.S. Department of Commerce. (2016). NIST Chemistry WebBook. http://webbook.nist.gov/chemistry/fluid

Vynnycky, M., Kimura, S., Kanev, K., & Pop, I. (1998). Forced convection heat transfer from a flat plate: The conjugate problem. International Journal of Heat and Mass Transfer, 41(1), 45-59.

Wang, T., & Luong, V. (1994). Hot-gas-side and coolant-side heat transfer in liquid rocket engine combustors. *Journal of Thermophysics and Heat Transfer, 8*(3), 524-530. doi:10.2514/3.574

Wang, Q., Wu, F., Zeng, M., Luo, L., Sun, J. (2006). Numerical simulation and optimization on heat transfer and fluid flow in cooling channel of liquid rocket engine thrust chamber. Engineering computations, Vol. 23 Iss 8, pp. 907-921.

Yang, V. (2004). Liquid rocket thrust chambers: Aspects of modeling, analysis, and design. Reston, VA: American Institute of Aeronautics and Astronautics.

Young, J. B., & Wilcock, R. C. (2002). Modeling the Air-Cooled Gas Turbine: Part 1—General Thermodynamics. *J. Turbomach. Journal of Turbomachinery, 124*(2), 207-213.

Young, J. B., & Wilcock, R. C. (2002). Modeling the Air-Cooled Gas Turbine: Part 2—Coolant Flows and Losses. *J. Turbomach. Journal of Turbomachinery, 124*(2), 214-221.

Zikanov, O. (2010). *Essential Computational Fluid Dynamics*. Hoboken, NJ: Wiley.

Zuckerman, N., & Lior, N. (2006). Jet Impingement Heat Transfer: Physics, Correlations, and Numerical Modeling. Advances in Heat Transfer, 565-631.

Zuckerman, N., & Lior, N. (2007). Radial Slot Jet Impingement Flow and Heat Transfer on a Cylindrical Target. Journal of Thermophysics and Heat Transfer, 21(3), 548-561.

A. Converged Model Residuals

a) Non-CHT: Air Impingement, 5.3 million cells

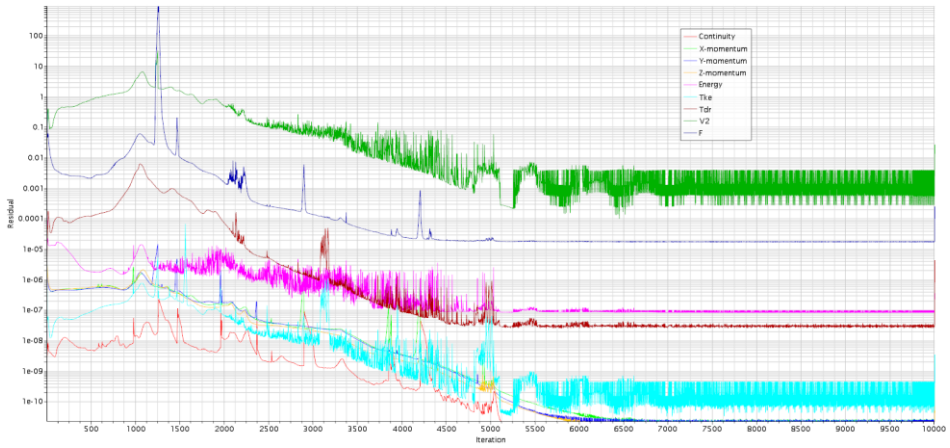

b) CHT: Air and Acrylic Impingement, 7.3 million cells

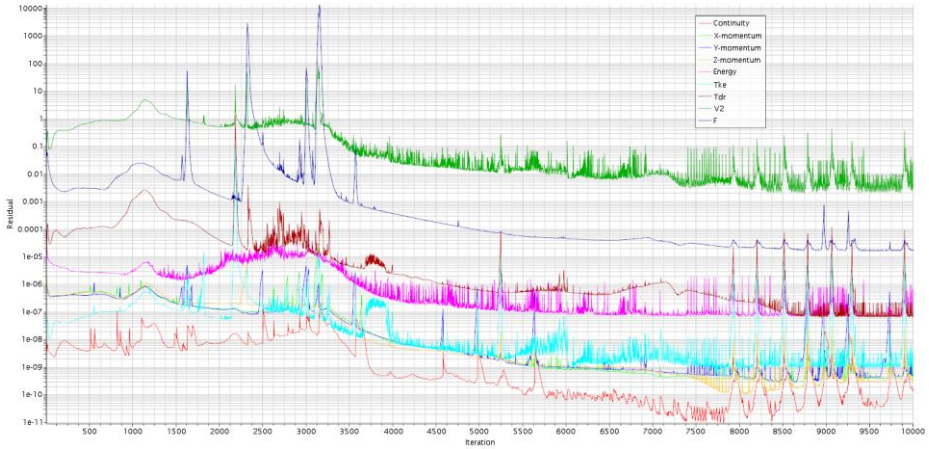

c) CHT: LH2 and SS 304 Impingement, 4.9 million cells

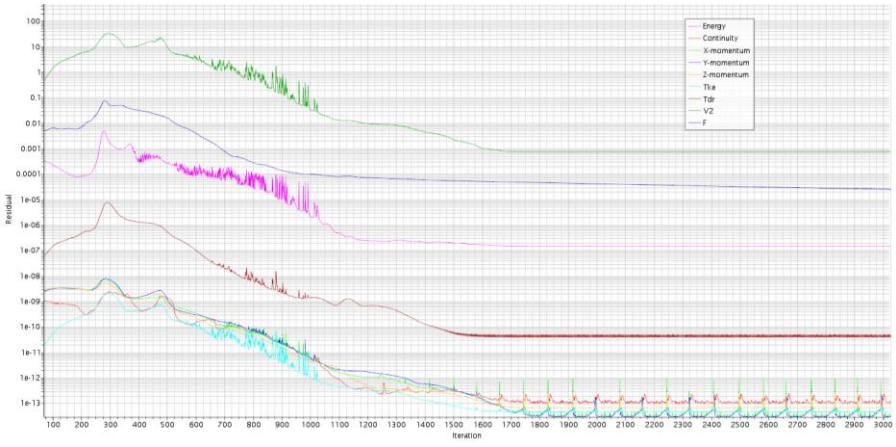

d) CHT: LH2 and Inconel x-750 Impingement, 4.9 million cells

e) CHT: LH2 and SS 304 Impingement & Film Cooling, 4.9 million cells

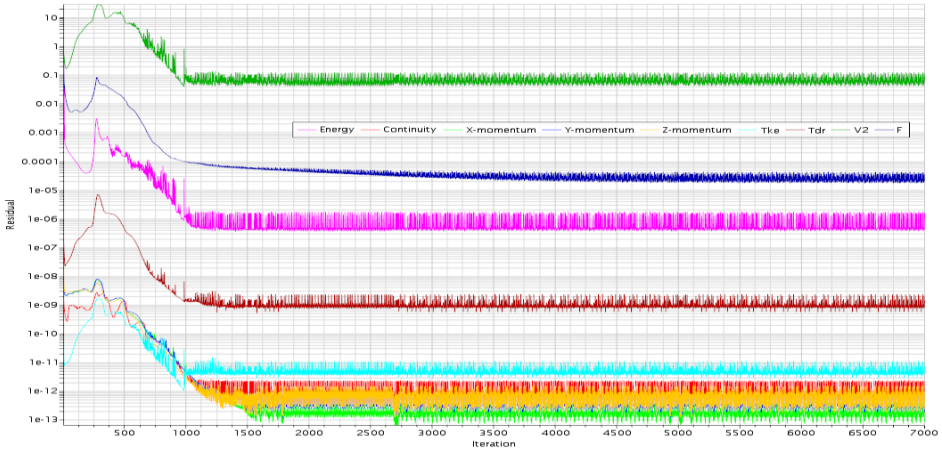

f) CHT: LH2 and Inconel x-750 Impingement & Film Cooling, 4.9 million cells

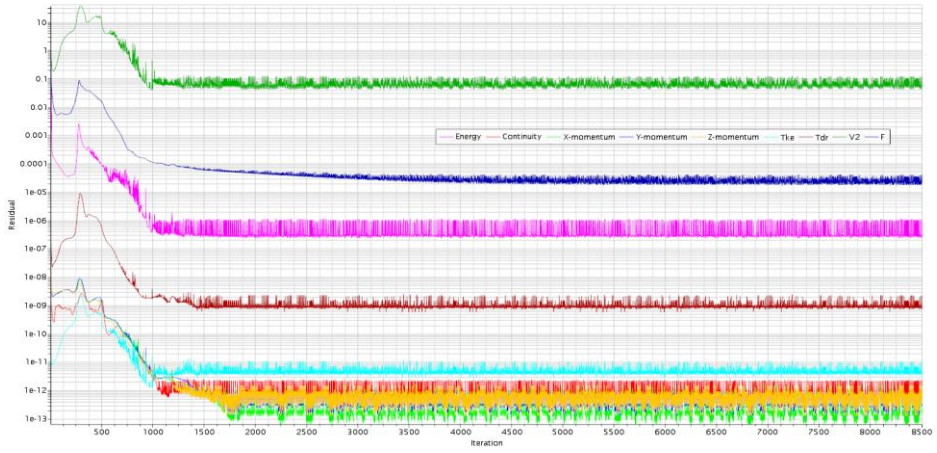

B. Full 360° Model Analysis

A) Mesh Model

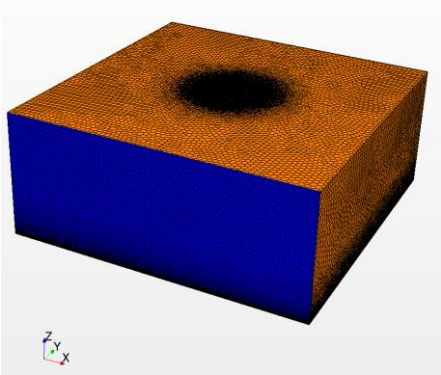

B) Converged Residual

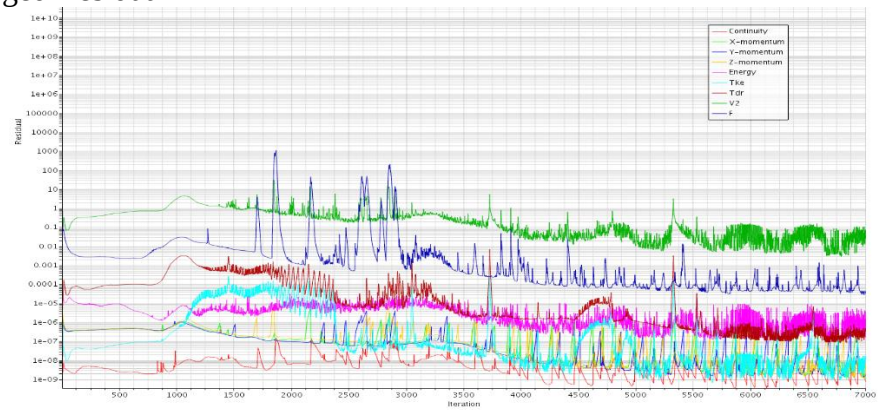

C) CFD

i) Nusselt Number Contour

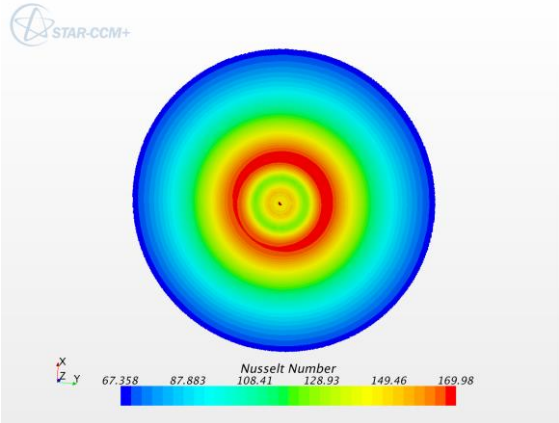

ii) Temperature Contour

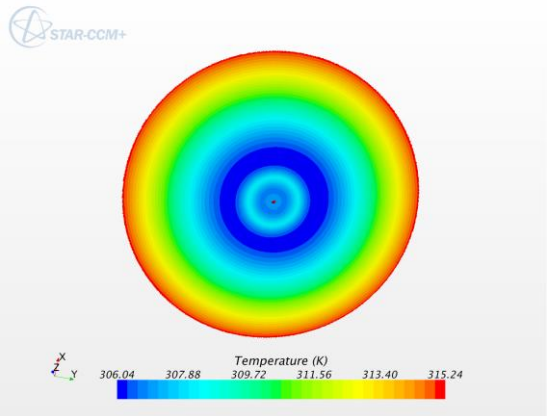

C. NASA CEA

```
    NASA-GLENN CHEMICAL EQUILIBRIUM PROGRAM CEA2, FEBRUARY 5, 2004
                  BY BONNIE MCBRIDE AND SANFORD GORDON
     REFS: NASA RP-1311, PART I, 1994 AND NASA RP-1311, PART II, 1996

 ***********************************************************************

 prob case=ERAU1133 ro equilibrium ions

  ! iac problem
 o/f 6.03
 p,bar  207
 supar 69
 reac
   fuel  H2(L) wt%=100. t,k=20.27
   oxid  O2(L) wt%=100. t,k=90.17
 output trans
 output    short
 output trace=1e-5
 end

             THEORETICAL ROCKET PERFORMANCE ASSUMING EQUILIBRIUM
           COMPOSITION DURING EXPANSION FROM INFINITE AREA COMBUSTOR

 Pin =  3002.3 PSIA
 CASE = ERAU1133

            REACTANT                        WT FRACTION      ENERGY
TEMP
                                             (SEE NOTE)     KJ/KG-MOL
K
 FUEL        H2(L)                           1.0000000     -9012.000
20.270
 OXIDANT     O2(L)                           1.0000000    -12979.000
90.170

 O/F=    6.03000  %FUEL= 14.224751  R,EQ.RATIO= 1.316199  PHI,EQ.RATIO=
1.316199

                CHAMBER   THROAT     EXIT
 Pinf/P           1.0000   1.7400   960.66
 P, BAR           207.00   118.97  0.21548
 T, K            3604.19  3387.87  1242.01
 RHO, KG/CU M  9.4378 0 5.8242 0 2.9571-2
 H, KJ/KG        -983.83 -2156.48 -10538.4
 U, KJ/KG       -3177.15 -4199.12 -11267.1
 G, KJ/KG       -62719.1 -60186.5 -31812.5
 S, KJ/(KG)(K)   17.1288  17.1288  17.1288

 M, (1/n)         13.663   13.790   14.172
 (dLV/dLP)t     -1.01936 -1.01447 -1.00000
 (dLV/dLT)p       1.3354   1.2666   1.0000
 Cp, KJ/(KG)(K)   7.3549   6.7393   2.9068
 GAMMAs           1.1471   1.1482   1.2529
 SON VEL,M/SEC    1586.1   1531.4    955.5
```

MACH NUMBER	0.000	1.000	4.575

TRANSPORT PROPERTIES (GASES ONLY)
CONDUCTIVITY IN UNITS OF MILLIWATTS/(CM)(K)

VISC,MILLIPOISE	1.0853	1.0371	0.46271

WITH EQUILIBRIUM REACTIONS

Cp, KJ/(KG)(K)	7.3549	6.7393	2.9068
CONDUCTIVITY	14.2864	12.4347	1.9072
PRANDTL NUMBER	0.5587	0.5621	0.7052

WITH FROZEN REACTIONS

Cp, KJ/(KG)(K)	3.7857	3.7507	2.9067
CONDUCTIVITY	5.7674	5.4273	1.9069
PRANDTL NUMBER	0.7124	0.7167	0.7053

PERFORMANCE PARAMETERS

Ae/At	1.0000	69.000
CSTAR, M/SEC	2320.8	2320.8
CF	0.6599	1.8836
Ivac, M/SEC	2865.2	4538.1
Isp, M/SEC	1531.4	4371.4

MOLE FRACTIONS

*H	2.5552-2	2.0503-2	4.4479-7
HO2	3.615 -5	1.710 -5	1.217-17
*H2	2.4429-1	2.4166-1	2.4024-1
H2O	6.8828-1	7.0726-1	7.5976-1
H2O2	1.764 -5	8.641 -6	2.465-15
*O	2.108 -3	1.287 -3	2.564-14
*OH	3.7450-2	2.7810-2	1.7023-8
*O2	2.272 -3	1.457 -3	4.044-14

* THERMODYNAMIC PROPERTIES FITTED TO 20000.K

NOTE. WEIGHT FRACTION OF FUEL IN TOTAL FUELS AND OF OXIDANT IN TOTAL OXIDANTS

.

D. NIST Isothermal Properties for Hydrogen

Values were extracted for T= 52.4 K. The markers indicate the values at 24 MPa.

Density:

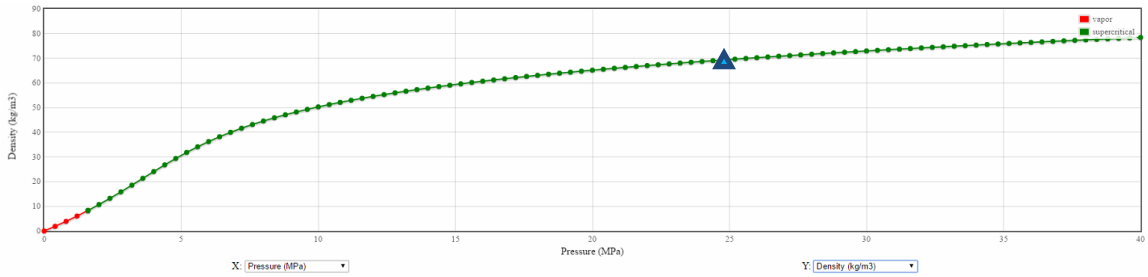

Specific Heat:

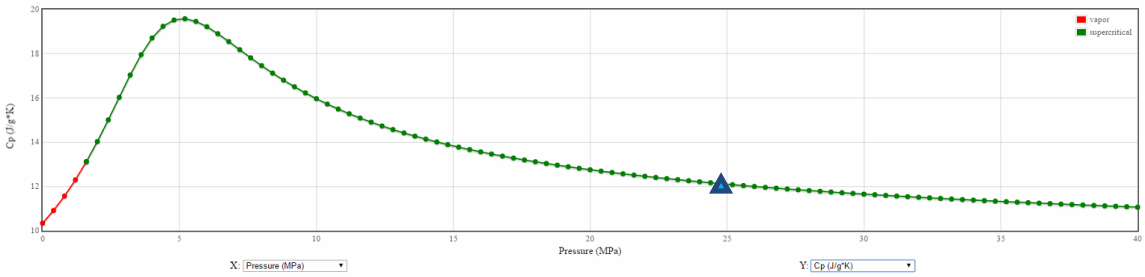

Viscosity:

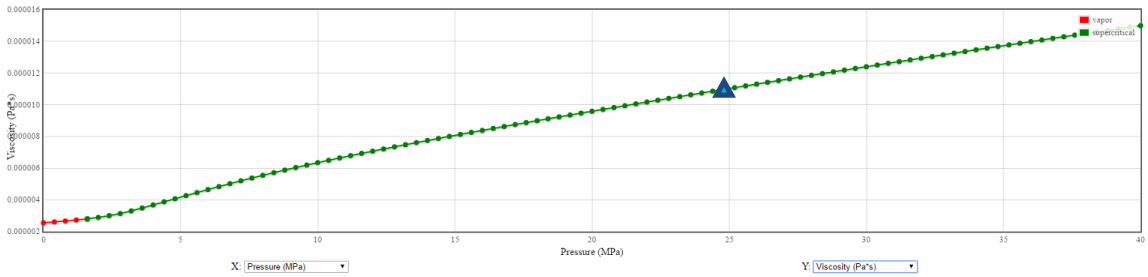

Thermal Conductivity: